

Similarities between the tropical Atlantic seasonal cycle and ENSO: An energetics perspective

N. J. Burls,¹ C. J. C. Reason,¹ P. Penven,^{1,2} and S. G. Philander^{1,3}

Received 24 March 2011; revised 1 September 2011; accepted 2 September 2011; published 10 November 2011.

[1] The tropical Pacific and Atlantic Oceans have similar mean states - easterly winds and a zonally sloping thermocline which shoals in the east - but strikingly different sea surface temperature variability. Seasonal and interannual variations have comparable amplitudes, and correspond to different modes of oscillation in the Pacific. In the Atlantic, the seasonal cycle is dominant and has properties of both those modes. The Bjerknes feedback between the wind and SST, and its associated delayed, negative feedback constitute a free (interannual) mode of the Pacific, but in the Atlantic influence the seasonal cycle. This difference between the two oceans is attributable to the smaller dimensions of the Atlantic. An energetic analysis shows a circular relationship between available potential energy and the work done by the wind from April until September in the Atlantic. This energetics perspective suggests that a seasonally excited thermocline mode of coupled variability plays an active role in the seasonal cycle during these months, after which point seasonal forcing regains control.

Citation: Burls, N. J., C. J. C. Reason, P. Penven, and S. G. Philander (2011), Similarities between the tropical Atlantic seasonal cycle and ENSO: An energetics perspective, *J. Geophys. Res.*, 116, C11010, doi:10.1029/2011JC007164.

1. Introduction

[2] Despite the dominant semi-annual signal in solar forcing at the top of the atmosphere, atmospheric and oceanic conditions in the central-eastern equatorial Pacific and Atlantic basins exhibit a distinct annual cycle so that conditions at the times of the two equinoxes are very different [Mitchell and Wallace, 1992]. Ocean-atmosphere interactions are of central importance to this seasonal cycle [Mitchell and Wallace, 1992; Xie and Philander, 1994; Xie, 1994; Chang and Philander, 1994]. In the tropics ocean-atmosphere interactions strongly influence climate variability at seasonal, interannual, and decadal time scales [Chang et al., 2006]. The equatorial regions support two distinct types of dynamic feedbacks; namely, the 'Bjerknes'/'thermocline' feedback and the 'Ekman'/'surface-layer' feedback [Neelin et al., 1998]. Both involve a circular argument whereby SST changes cause and also respond to wind perturbations. The shallow thermocline in the east permits SST to be strongly influenced by the vertical advection of colder subsurface water across the thermocline. The extent of cooling associated with this vertical advection depends on the strength of vertical velocities induced by local Ekman pumping (which support the Ekman feedback) and on remotely forced changes in the thermocline depth induced

by a basin wide adjustment to wind stress fluctuations (which support the Bjerknes feedback). These feedbacks amplify the response to initially modest wind fluctuations and thus have significant effects on the atmospheric and oceanic circulations.

[3] A clear distinction exists in the central-eastern equatorial Pacific between the mechanisms that determine interannual variability and those that determine the seasonal cycle. Interannual SST variability in the eastern-central Pacific is primarily driven by equatorial upwelling acting on thermocline displacements as the Bjerknes feedback leads to the growth of the anomalous conditions associated with El Niño and the Southern Oscillation (ENSO) [Bjerknes, 1969]. Conceptually there are two main idealized modes presented in the literature to account for the oscillatory nature of interannual SST variability within the Pacific. Both the delayed oscillator [Hirst, 1986; Suarez and Schopf, 1988; Neelin et al., 1998] and recharge oscillator [Jin, 1997] paradigms attribute the growth of interannual SST anomalies to the Bjerknes feedback. They differ however in their description of the phase transition mechanism which leads to the periodic nature of ENSO. For the delayed oscillator idealization, the phase-transition mechanism is attributed to the reflection, at the western edge of the basin, of off-equatorial Rossby waves generated during the initial growth phase and so the delayed oscillator mode has a timescale which depends on the processes of oceanic adjustment [Hirst, 1986; Suarez and Schopf, 1988; Neelin et al., 1998]. In the case of the recharge oscillator idealization, ocean wave propagation process is not at the centre of the delayed negative feedback, but rather regarded as a part of the oceanic adjustment in which heat and mass are re-distributed under changing wind forcing. The recharge-discharge of equatorial

¹Department of Oceanography, University of Cape Town, Cape Town, South Africa.

²LPO, UMR 6523 CNRS, IFREMER, IRD, UBO, LMI ICEMASA, Plouzane, France.

³Geophysical Fluid Dynamics Laboratory, Princeton University, Princeton, New Jersey, USA.

zonal mean heat content is viewed as the phase-transition mechanism [Jin, 1997].

[4] In contrast to interannual variability, seasonal SST variability in the eastern-central Pacific is primarily attributed to the Ekman feedback mechanism and its associated SST-modes [Chang and Philander, 1994]. Although seasonal variations in the thermocline depth have a large amplitude north of the equator, the thermocline depth along the equator does not vary much seasonally in the Pacific [McPhaden *et al.*, 1998] with the largest seasonal temperature variations confined to the surface mixed layer [McPhaden *et al.*, 1998]. As many studies have shown, seasonal SST changes in the cold tongue region are highly correlated with local winds [Hayes *et al.*, 1991; Chang, 1993, 1994; Swenson and Hansen, 1999; Wang and McPhaden, 1999].

[5] Seasonal variations in the intensity of the local winds and associated Ekman pumping are thought to be controlled by equatorially antisymmetric and equatorially symmetric SST-modes which govern the seasonal cycle where the equatorial thermocline is shallow [Chang and Philander, 1994]. These unstable coupled modes are forced by the local Ekman feedback mechanism and do not involve remotely forced changes in thermocline depth [Neelin *et al.*, 1998; Neelin, 1991]. The Ekman feedback involves a purely local dynamical ocean response to changes in the wind forcing. Like the Bjerknes feedback, SST anomalies modify the strength of equatorial winds, which then act to reinforce the original SST anomaly. However, unlike the Bjerknes feedback mechanism, thermocline depth variations associated with the Ekman feedback mechanism are driven by the divergence of surface Ekman currents rather than remotely forced geostrophic current anomalies [Chang and Philander, 1994].

[6] In the equatorial Atlantic, the primary feedback mechanism deemed responsible for the seasonal evolution of coupled conditions and the development of the cold tongue is thought to be equivalent to that responsible for the seasonal development of the cold tongue in the Pacific. Seasonal fluctuations in central-eastern basin equatorial SST have similarly been attributed to seasonally excited SST-modes and their associated Ekman feedback [Chang and Philander, 1994]. The annual re-establishment of the equatorial cold tongue commences in April/May when equatorial SSTs start to cool. The initiation of this cooling is attributed to the movement of continental convection from the equator into the Northern Hemisphere, and hence accelerating the southerly winds over the Gulf of Guinea [Mitchell and Wallace, 1992; Okumura and Xie, 2004]. These cross-equatorial southerly winds drive upwelling south of the equator cooling the eastern equatorial Atlantic. As in the Pacific, a zero frequency, zero zonal wave number asymmetric SST-mode with a rapid growth rate is accredited with the sudden seasonal growth in asymmetric conditions about the equator, as an unstable cross-equatorial Ekman feedback mechanism leads to the growth of the equatorial cold tongue-Intertropical Convergence Zone (ITCZ) complex [Chang and Philander, 1994].

[7] However, unlike in the equatorial Pacific where interannual fluctuations in central-eastern basin SST are of a similar magnitude to seasonal fluctuations, seasonal SST variability dominates in the Atlantic [Vauclair and du Penhoat, 2001; Xie and Carton, 2004]. Moreover, the largest fluctuations

in thermocline depth along the equator occur interannually in the Pacific [McPhaden *et al.*, 1998] but seasonally in the Atlantic [Merle, 1980; Vauclair and du Penhoat, 2001; Schouten *et al.*, 2005]. These distinctions between the two basins are highlighted in section 3.1 and beg the question - Why do interannual SST and thermocline depth fluctuations dominate over seasonal fluctuations in the central-eastern Pacific while the opposite is true in the Atlantic?

[8] Previous studies have attributed the relatively small amplitude of interannual variability seen in the Atlantic to the smaller basin size, the different distribution of land masses, and the fact that there is no permanent equatorial warm pool or equatorial convection in the Atlantic [Zebiak, 1993; Keenlyside and Latif, 2007]. The small amplitude of interannual variability in the equatorial Atlantic has also been attributed to a delayed negative feedback from equatorial waves that interrupts the positive ocean-atmosphere coupling during boreal summer [Foltz and McPhaden, 2010a, 2010b]. A different perspective offered by the analysis conducted within this paper is that, unlike the Pacific, the seasonal cycle in the Atlantic involves the Bjerknes mechanism and the delayed, ocean memory, negative feedback mechanism and therefore the seasonal signal dominates. In their study of the seasonal cycle in the equatorial Atlantic, Ding *et al.* [2009] suggest that the relationship between SST, thermocline depth and surface zonal currents is more consistent with a 'thermocline mode' than a SST-mode. The analysis undertaken in this paper substantiates this suggestion. The hypothesis put forward here is that the seasonal cycle in the Atlantic involves not only an asymmetric SST-mode excited as the cold tongue develops, but also a superimposed thermocline mode.

[9] This paper is structured as follows. The next section (section 2) details the data and methods employed within this study. In section 3, the results in support of the hypothesis outlined above are presented in three subsections: the first (section 3.1) capitalizes on the vast knowledge gained in the tropical Pacific by comparing the nature of variability in a number of pertinent variables in the Atlantic and Pacific; the second (section 3.2) shows that all the elements of the Bjerknes are seasonally active within the Atlantic; finally section 3.3 quantifies the delayed, negative feedback mechanism responsible for the seasonal decay of the Bjerknes feedback. As discussed in section 4, the analysis put forward in section 3 supports the perspective that the northward movement of ITCZ (as the cold tongue starts to develop in the Atlantic) along with the Bjerknes feedback, allow the equatorial trade winds to intensify until, from August into October, a delayed, ocean memory mechanism reverses the growth phase. Section 5 summarizes the results.

2. Data and Methods

2.1. Data

[10] The analysis conducted within this study is based primarily on two data sets.

[11] 1. For the Atlantic-Pacific comparison conducted in section 3.1, monthly temperature and salinity fields from the 1/2° Simple Ocean Data Assimilation (SODA) re-analysis product [Carton and Giese, 2008], spanning 47 years

(1958–2004), have been used to assess equatorial Atlantic and Pacific Available Potential Energy (APE) and Background Potential Energy (BPE). Density values have been calculated using a non-linear equation of state [Jackett and McDougall, 1995].

[12] 2. To facilitate the analysis focused on the Atlantic in sections 3.2 and 3.3, a simulation of oceanic conditions within the tropical Atlantic between 1980 and 2004 has been conducted using the Regional Ocean Modeling System (ROMS), hereafter referred to as ROMS-TAtl. ROMS is a split-explicit, free-surface, sigma (terrain-following) coordinate ocean model based on the primitive equations with the Boussinesq and hydrostatic approximations made [Shchepetkin and McWilliams, 2005]. This simulation was undertaken to acquire the temperature, salinity and momentum evolution equations tendency terms required to evaluate the processes determining APE and BPE evolution in sections 3.2.1 and 3.3 and for the surface layer heat budget analysis conducted in section 3.2.2.

[13] The ROMS-TAtl simulation has a Mercator grid extending zonally from 60°W–15°E and meridionally from 10°S–14°N with a horizontal resolution of $\sim 1/6^\circ$. After some experimentation with the meridional extent of this domain the northern and southern open boundaries were chosen such that the domain was large enough to resolve all the relevant features within the equatorial Atlantic but still small enough for the equatorial thermocline to be adequately constrained by the prescribed lateral boundary conditions (it was found that the larger the chosen domain the more diffuse the equatorial thermocline). The adaptive algorithm of Marchesiello *et al.* [2001], where inward and outward information fluxes at the open boundaries are treated separately, was used to deal with the open boundaries. Inward fluxes were nudged towards external data with prescribed surface elevation, barotropic horizontal velocity, baroclinic horizontal velocity, temperature and salinity provided by the SODA re-analysis product [Carton *et al.*, 2000; Carton and Giese, 2008]. Surface vertical boundary conditions were provided by bulk surface fluxes derived from atmospheric parameters supplied by the NCEP-DOE II, re-analysis product [Kanamitsu *et al.*, 2002]. The simulation was spun up for 10 years using lateral and surface boundary conditions for 1980, the first year of the simulation period. Thereafter the model was forced with interannually varying surface and lateral boundary conditions from 1980–2004. For a more detailed description and validation of the ROMS-TAtl configuration, see Burls [2010].

[14] Other data sets employed in this paper are, the Pilot Research Moored Array in the Tropical Atlantic (PIRATA) mooring data [Servain *et al.*, 1998] and the surface current climatology product of Lumpkin and Garraffo [2005].

2.2. Energetics Analysis

[15] In this study, oceanic variability is viewed from an energetics perspective. APE and BPE are the energetic quantities of interest as they provide a concise evaluation of basin wide changes in zonal thermocline slope and mean thermocline depth in response to large scale atmospheric forcing. In the Pacific, energetics analysis of interannual variability has elucidated the mechanisms through which ocean-atmosphere interactions give rise to ENSO [Goddard and Philander, 2000; Fedorov *et al.*, 2003; Fedorov, 2007].

interannual SST fluctuations in the central-eastern equatorial Pacific are highly anti-correlated with the amount of gravitational APE in the equatorial Pacific [Goddard and Philander, 2000]. This inverse relationship arises from the fact that APE effectively represents changes in east-west slope of the equatorial thermocline. During La Niña, the east-west slope of the thermocline is at a maximum together with equatorial Pacific APE, while during El Niño conditions, APE and the slope of the thermocline are at a minimum. Thus, the equatorial Pacific ocean gains APE during the transition from El Niño to La Niña and loses APE during the transition from La Niña to El Niño. Interannual SST anomalies in the Pacific can therefore be regarded as surface expressions of upper ocean energy changes [Goddard and Philander, 2000]. By examining the processes by which the tropical Pacific Ocean gains and redistributes energy, Goddard and Philander [2000] were able to test the delayed oscillator theory [Battisti, 1988; Suarez and Schopf, 1988; Battisti and Hirst, 1989]. Here, an investigation into the mechanisms driving seasonal APE and BPE changes provides us with insight into the role of the ocean within equatorial Atlantic ocean-atmosphere interactions occurring at seasonal timescales.

[16] Formalized by Lorenz [1955], the available potential energy of a fluid volume is defined as the difference in Potential Energy (PE) between its physical state and a rest state of minimum potential energy

$$APE = \int \int \int g \rho z dV - \int \int \int g \rho_r z_* dV, \quad (1)$$

where g is the acceleration due to gravity, $\int \int \int g \rho z dV$ is the physical PE of the fluid volume and $\int \int \int g \rho_r z_* dV$ the minimum PE attainable within the fluid volume: a rest state in which all density surfaces are level. For the fluid parcel at position (\mathbf{x}, t) and depth z with density ρ , $z_*(\mathbf{x}, t)$ is its vertical position and $\rho_r(\mathbf{x}, t)$ its density in the reference state of minimum PE. In the oceanic context the fluid is assumed incompressible and so the effect of pressure on density during the leveling process is neglected ($\rho_r = \rho$) [Oort *et al.*, 1989; Huang, 1998]. Therefore,

$$\begin{aligned} APE &= \underbrace{\int \int \int g \rho z dV}_{PE} - \underbrace{\int \int \int g \rho z_* dV}_{BPE} \\ &= \int \int \int g \rho (z - z_*) dV, \end{aligned} \quad (2)$$

where $\int \int \int g \rho z dV$ is the physical PE of the fluid volume and $\int \int \int g \rho z_* dV$ the minimum PE attainable through the reversible adiabatic redistribution of mass, referred to as the BPE. The vertical position of each water parcel in the rest state, $z_*(\mathbf{x}, t)$, is determined following Huang [1998]. $V(\mathbf{x}, t)$ is the volume beneath the center of the fluid parcel, $\rho(\mathbf{x}, t)$, once moved to its rest state position according to $V(\mathbf{x}, t) = \int \int \int H(\rho(\mathbf{x}', t) - \rho(\mathbf{x}, t)) dV'$, where H is a Heaviside step function, satisfying $H(y) = 0$ for $y < 0$, $H(y) = 0.5$ for $y = 0$ and $H(y) = 1$ for $y > 0$ [Winters *et al.*, 1995; Huang, 1998]. The corresponding vertical co-ordinate $z_*(\mathbf{x}, t) = z(V(\mathbf{x}, t))$ is then found based on the fact that the volume above the bottom of the chosen domain is a function of z [Huang, 1998].

[17] Previous studies of equatorial energetics in the Pacific [Goddard and Philander, 2000; Fedorov et al., 2003; Fedorov, 2007] have used an approximation for APE that assumes the background rest state is stably stratified and that density perturbations relative to the reference density profile are small in amplitude. APE can then be described by its leading order Taylor-expanded term [Reid et al., 1981; Oort et al., 1989]. A second assumption made in the previous literature when employing this definition for APE is that the background rest state (the BPE of the fluid volume) is fixed in time. This assumption facilitates the derivation of an evolution equation for APE defined by its leading order Taylor-expanded term [Goddard and Philander, 2000, Appendix]. However, this assumption is only valid if changes in the mass and stratification of the chosen volume are negligible over the timescales for which one is assessing APE changes. As outlined by Burls [2010], although the assumption that BPE changes are small may hold when evaluating interannual variability in tropical Pacific (15°N–15°S 130°E–85°W 0–400 m) APE, it does not appear to hold when evaluating APE changes within the equatorial (3°S–3°N 60°W–15°E 0–400 m) and tropical (8°S–8°N 60°W–15°E 0–400 m) Atlantic on seasonal to interannual timescales. Since the interest here is mainly on seasonal equatorial Atlantic APE changes, the approximation of APE used in the previous work is avoided and APE is evaluated using equation (2) which takes into account BPE changes.

[18] The evolution equations employed in sections 3.2.1 and 3.3 when evaluating the processes determining APE and BPE evolution within an open boundary equatorial Atlantic domain are given in Appendix A. A linear equation of state has been used to approximate density values from simulated ROMS-TAtl temperature and salinity fields (which observe the tracer conservation equation). The use of a linear equation of state ensures that the density field is conserved. This linear approximation is shown to be valid by Burls [2010]. A percentage difference of 21% exists between the mean of equatorial Atlantic APE values calculated using a density field derived with a linear equation of state and the mean of APE values calculated using a non-linear equation of state. Variability within the two time series is however very similar with a correlation coefficient of 0.99 and a standard deviation of 2.09×10^{16} J for the linear equation of state time series and 2.04×10^{16} J for the non-linear equation of state time series. These statistics indicate that the difference between the two APE time series results largely form a constant bias associated with the fact that the effect of pressure is neglected in the density field calculated using an equation of state linearized around a constant background density.

[19] APE and BPE are nonlinear terms and in calculating their climatological values the climatological average of the product of interannual perturbations is neglected as the contribution of this term is seen to be small [Burls, 2010]

$$APE_{cl} \sim \int \int \int g \rho_{cl} (z - z_{*cl}) dV \quad (3)$$

$$BPE_{cl} \sim \int \int \int g \rho_{cl} z_{*cl} dV. \quad (4)$$

2.3. Surface Layer Heat Budget

[20] In section 3.2.2, surface layer heat budgets for the Atl3 region (3°S–3°N 20°W–0°E) have been calculated. The relative contribution of each process in forcing the temporal evolution of the mean temperature (\bar{T}) within a surface layer of depth $h(t, x, y)$, $\frac{\partial \bar{T}}{\partial t}$, has been quantified by deriving an evolution equation (equation (5)) as with Vialard and Delecluse [1998] and Menkes et al. [2006]

$$\begin{aligned} \frac{\partial \bar{T}}{\partial t} = & - \underbrace{\frac{1}{h} \int_{-h}^0 u \frac{\partial T}{\partial x} dz}_{A_x} - \underbrace{\frac{1}{h} \int_{-h}^0 v \frac{\partial T}{\partial y} dz}_{A_y} - \underbrace{\frac{1}{h} \int_{-h}^0 w \frac{\partial T}{\partial z} dz}_{A_z} \\ & + \underbrace{\frac{1}{h} \int_{-h}^0 K_{th} \nabla^2 T dz}_{D_h} - \underbrace{\frac{1}{h} \left(K_{tv} \frac{\partial T}{\partial z} \right)_{z=-h}}_V - \underbrace{\frac{1}{h} \frac{\partial h}{\partial t} (\bar{T} - T_{z=-h})}_E \\ & + \underbrace{\frac{q_* + q_s(1 - f_{z=-h})}{h \rho_o C_p}}_F, \end{aligned} \quad (5)$$

where $T_{z=-h}$ is the temperature at the base of the chosen surface layer, K_{th} represents the horizontal temperature diffusion coefficient, K_{tv} the vertical temperature diffusion coefficient, u and v the horizontal velocity components, w the vertical velocity component, q_s the surface solar radiative flux, $f(z)$ the fraction of solar radiation reaching depth z and q_* is the non penetrative part of the surface heat flux that consists of the net long-wave radiative flux, the latent heat flux and the sensible heat flux components. Each term represents a physical process which may contribute to the variability of the mean temperature (\bar{T}) within the chosen surface layer: zonal advection A_x , meridional advection A_y , vertical advection A_z , horizontal diffusion D_h , vertical mixing V at the base of the layer, entrainment E at the base of the layer and the surface heat flux forcing F . Two day averages of each term within the ROMS-TAtl temperature evolution equation has been vertically integrating over the chosen surface layer depth and a 14 day running mean has then been applied to each time series to smooth out the high frequency variability.

[21] Two different surface layer definitions are used in order to identify the relative contribution of each surface layer process to seasonal SST variability within the central-eastern equatorial Atlantic. There are as follows:

[22] 1. The Surface Mixed Layer (SML), the depth of which, $h(t,x,y)$, is defined according to the mixed layer depth criterion of Lorbacher et al. [2006]. As opposed to defining the mixed layer depth as the depth at which temperature has decreased by a certain amount from its surface value, this mixed layer depth criterion is based on the shallowest extreme curvature of near surface layer temperature profiles and deals better with a data set that has varying vertical resolutions as well as a large variety of observed stratification profiles.

[23] 2. A deeper layer of fixed depth, $h = 70$ m, referred to as the Warm Water Layer (WWL) which corresponds to the mean depth of the thermocline over the Atl3 region.

[24] The reason behind conducting a heat budget for the WWL as well as the SML is to resolve the role of vertical advection in seasonal SST changes.

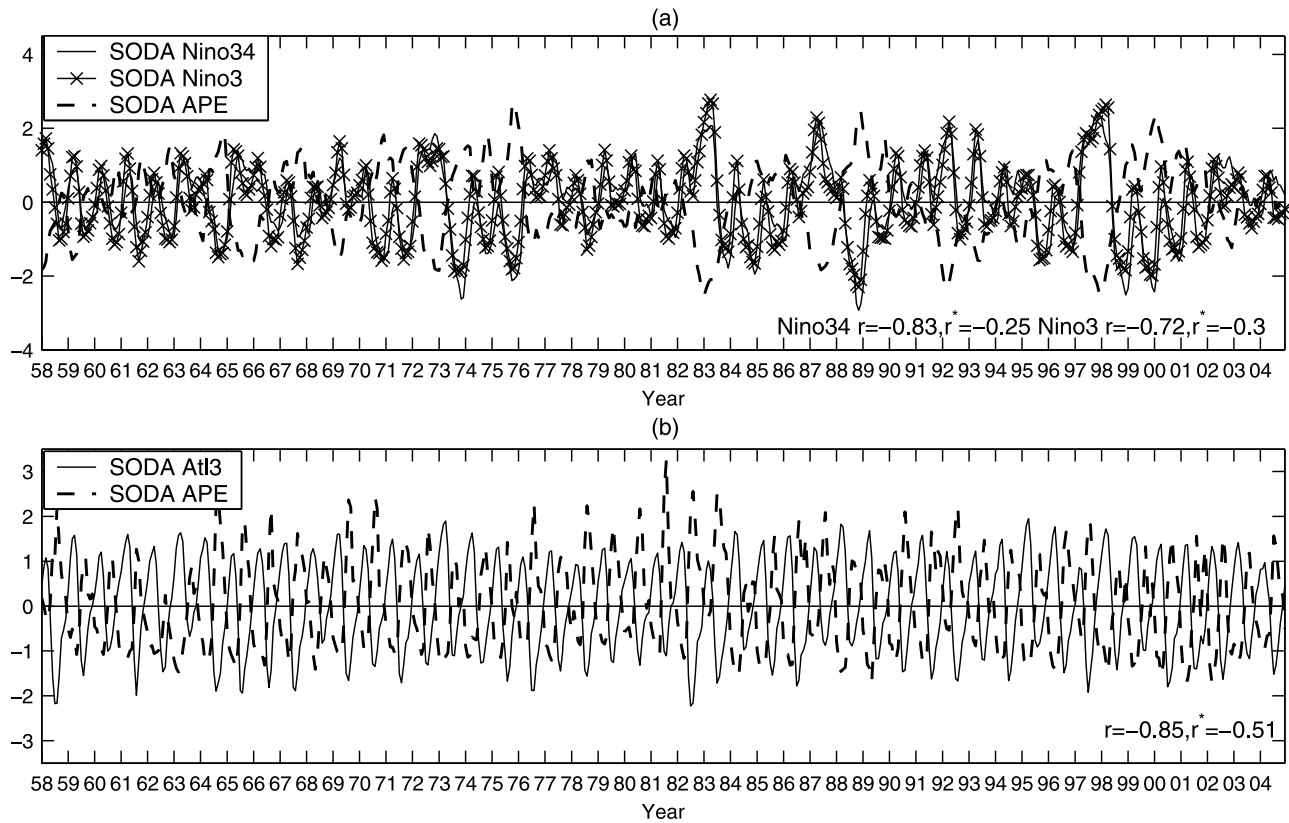


Figure 1. (a) A comparison between total Niño 3.4 (5°N – 5°S 170°W – 120°W) SST, Niño 3 (5°N – 5°S 150°W – 90°W) SST and equatorial Pacific (5°N – 5°S 130°E – 85°W 0–400 m) APE fluctuations. (b) A comparison between total Atl3 (3°S – 3°N 20°W – 0°E) SST and equatorial Atlantic (3°S – 3°N 60°W – 15°E 0–400 m) APE fluctuations. The correlation between each SST index and APE values (r) is given on each figure, together with the required correlation value for significance at the 95% level taking into account the effective degrees of freedom (r^*). SST indices and APE values were calculated using SODA data and have been normalized and detrended.

[25] At each ROMS-TAtl grid point, two day averages of the wind stress forcing have been used to estimate vertical velocities at the base of the Ekman layer induced by local wind driven Ekman divergence (here after referred to as the Ekman vertical velocity W_E). A previously used method [Zebiak and Cane, 1987; Sterl and Hazeleger, 2003; Okumura and Xie, 2004; Barreiro et al., 2005] is employed to estimate the Ekman layer transports near the equator. As in the literature, a value of 0.5 d^{-1} is given to the linear friction term. This term is introduced since $f \rightarrow 0$ at the equator and represents the loss of energy due to shear stresses within the surface currents. The Ekman vertical velocities calculated for each grid point in the horizontal plane were then area averaged over the Atl3 region to provide a measure of the intensity of locally forced Ekman pumping for the Atl3 region.

3. Results

3.1. Pacific Versus Atlantic SST-APE Relationship

[26] Using SODA data, this section compares the nature of central-eastern basin SST, equatorial APE, equatorial BPE and western-central basin wind stress fluctuations in the Pacific and Atlantic basins.

[27] For the Pacific and Atlantic respectively, Figure 1 depicts the relationship between total values in equatorial APE and central-eastern basin SST indices that capture the essence of the variability in each basin. (“Total” refers to the combined seasonal and interannual signals.) Commonly used indices are the Atl3 (3°S – 3°N 20°W – 0°E) SST for the Atlantic and the Niño3.4 (5°N – 5°S 170°W – 120°W) and Niño3 (5°N – 5°S 150°W – 90°W) SST for the Pacific. The narrower meridional extent of the domain over which equatorial Atlantic APE is evaluated (3°S – 3°N) in comparison to the Pacific (5°S – 5°N) is due to the narrower meridional extent of the SST variability associated with the zonal mode.

[28] Consistent with previous results, Figure 1a shows that Niño3.4 and Niño3 SST fluctuations are highly anti-correlated with equatorial Pacific APE. A correlation coefficient of $r = -0.83$ ($r^* = -0.25$) is seen between Niño3.4 SST and equatorial APE and one of $r = -0.72$ ($r^* = -0.3$) is seen between Niño3 SST and equatorial APE (Figure 1a). (Here r^* represents the required correlation value for significance at the 95% level taking into account the effective degrees of freedom.) The correlation between these Pacific SST indices and APE is even greater when interannual anomalies with respect to climatological values are considered. A correlation coefficient of $r = -0.87$ ($r^* = -0.25$) is seen between

anomalous Niño3.4 SST and equatorial APE and a correlation coefficient of $r = -0.87$ ($r^* = -0.25$) is seen between the anomalous Niño3 SST and equatorial APE (not shown).

[29] The robust relationship between central-eastern basin SST and equatorial APE observed in the Pacific is also seen to be present in the Atlantic basin. A correlation coefficient of $r = -0.85$ ($r^* = -0.51$) is seen between Atl3 SST and equatorial APE (Figure 1b). This result is not surprising considering that both equatorial basins are characterized by a mean state comprising of easterly wind stress and a zonally sloping thermocline which shoals in the east. The presence of a strong SST-APE relationship in the Atlantic, like that observed in the Pacific, suggests that anomalous vertical advection in the central-eastern basin resulting from thermocline depth changes associated with the large scale redistribution of warm surface water, plays an equally important role in determining SST variability in the Atlantic as it does in the Pacific.

[30] However, when comparing Figures 2a and 2b, which show the magnitude of total APE changes versus climatological APE changes in the equatorial Pacific and Atlantic respectively, it is evident that the biggest distinction between these two basins exists in the period of dominant APE fluctuations. While the largest changes in APE occur on interannual timescales in the Pacific, the largest changes in APE occur annually in the Atlantic. The east-west tilt of the thermocline [McPhaden *et al.*, 1998] and therefore APE [Fedorov, 2007] hardly varies seasonally in the Pacific, whereas large seasonal variations in the zonal slope of the thermocline are observed in the Atlantic [Merle, 1980; Vaucclair and du Penhoat, 2001; Schouten *et al.*, 2005].

[31] Likewise, the largest fluctuations in central-eastern basin equatorial SST, equatorial BPE and western-central basin wind stress occur on interannual timescale in the Pacific and on seasonal timescales in the Atlantic, as shown in Figures 2c–2h. It is suggested here that this distinction between the two basins in terms of the timescale of dominant APE, SST, BPE and wind stress fluctuations is due to the fact that while the Bjerknes feedback and the delayed, negative feedback mechanism act on interannual timescales in the Pacific, they act on seasonal timescales in the Atlantic. The results presented in the following two sections provide evidence that both the Bjerknes feedback (section 3.2) and the delayed, ocean memory, negative feedback mechanism (section 3.3) are seasonally active in the Atlantic.

[32] Atlantic APE has been evaluated over domains of differing meridional extent. Meridionally extending the domain does not have a significant effect on the signature of APE variability, the seasonal signal remains dominant [Burls, 2010]. APE fluctuations for the domain extending from 3°S–3°N correlate best with Atl3 SST changes at zero lag (Figure 1b). APE values for domains extending to 5°S–5°N, 8°S–8°N and 15°S–15°N correlate best with Atl3 SST changes at one month lag [Burls, 2010]. The strength of this one month lagged correlation decreases as the meridional extent increases. The fact that the APE values for the larger domains correlate best with Atl3 SST changes at one month lag is thought to be due to the fact that these larger domains take longer to adjust to seasonal changes in the wind forcing due to the slower phase speed of off equatorial Rossby waves in comparison to equatorial Kelvin waves.

3.2. The Seasonally Excited Bjerknes Feedback

[33] The analysis conducted within this section is based on the ROMS-TAtl simulation and seeks to substantiate the suggestion that the Bjerknes feedback is seasonally active within the Atlantic. Supporting the concept that the Bjerknes feedback mechanism is excited seasonally requires evidence that all three components of the Bjerknes feedback mechanism participate in the development of the cold tongue; namely, (1) an atmospheric response to eastern equatorial SST changes that results in wind changes to the west, (2) the creation of heat content changes in the east by wind changes in the west, (3) the translation of thermocline depth fluctuations in the central-eastern equatorial basin into SST changes.

[34] Concerning the first element of the Bjerknes feedback mechanism, the spatial pattern in the correlation between climatological zonal wind stress and Atl3 SST suggests that, like the interannual scenario in the Pacific, easterlies in the western equatorial Atlantic are sensitive to seasonal Atl3 SST changes and hence that the first element of the Bjerknes feedback mechanism is seasonally active. Seasonal, central-eastern basin SST changes correlate best not with local zonal wind stress changes, but with changes in zonal wind stress to the west (40°W–18°W $r > 0.9$) [Burls, 2010]. Furthermore, the sensitivity of the seasonal development of zonal winds in the western-central equatorial Atlantic to zonal SST gradients which develop as a result of the seasonal development of the cold tongue has been demonstrated by Okumura and Xie [2004]. The analysis conducted here therefore focuses on the oceanic component of the coupled system.

3.2.1. The Mechanisms Driving Seasonal Changes in Central-Eastern Basin Heat Content

[35] To ascertain whether the second element of the Bjerknes feedback is associated with the seasonal development of the cold tongue, this section investigates the mechanisms driving eastern basin heat content changes by following changes in the zonal slope of the thermocline (APE). The processes dictating seasonal, equatorial Atlantic (3°S–3°N 60°W–15°E 0–400 m) and tropical Atlantic (8°S–8°N 60°W–15°E 0–400 m) APE changes are established by evaluating the various terms in the APE evolution equation as outlined in section 2.2 and Appendix A. Several observational and modeling studies have investigated the dynamical adjustment of the upper equatorial Atlantic in response to seasonal wind forcing [Adamec and O'Brien, 1978; Merle, 1980; Busalacchi and Picaut, 1983; du Penhoat and Treguier, 1985; Weisberg and Tang, 1985, 1987, 1990; Philander and Pacanowski, 1986a; Schouten *et al.*, 2005; Ding *et al.*, 2009]. However, the energetics analysis presented here offers a unique perspective as it quantifies the influence that seasonal oceanic adjustment has on the coupled system via its influence on the ability of seasonal wind forcing to do work on the ocean.

[36] Figures 3a and 3b depict the climatological balance of terms for the APE evolution equation (equation (A1)), assessed over the equatorial and tropical Atlantic domains. Clearly evident in these figures is the fact that seasonal APE changes are driven primarily by the buoyancy power term. This result is consistent with that of Goddard and Philander [2000] who find the dominant term driving large interannual

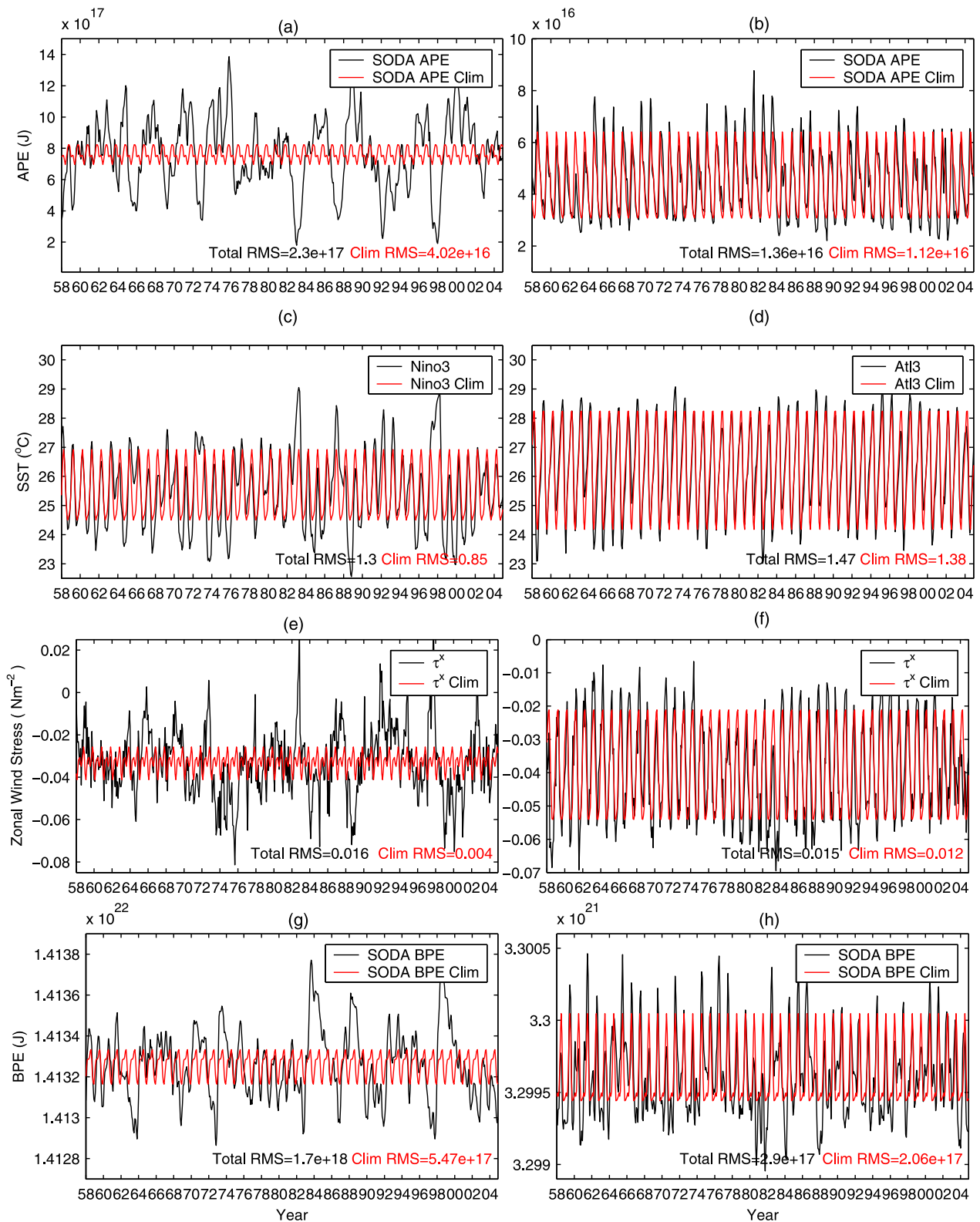


Figure 2. A comparison between variability in total versus climatological (a) equatorial Pacific (5°N–5°S 130°E–85°W 0–400 m) APE, (b) equatorial Atlantic (3°S–3°N 60°W–15°E 0–400 m) APE, (c) Niño 3 (5°N–5°S 150°W–90°W) SST, (d) Atl3 (3°S–3°N 20°W–0°E) SST, (e) western–central Pacific zonal wind stress (5°N–5°S 160°E–160°W), (f) western Atlantic zonal wind stress (3°S–3°N 40°W–20°W), (g) equatorial Pacific (5°N–5°S 130°E–85°W 0–400 m) BPE and (h) equatorial Atlantic (3°S–3°N 60°W–15°E 0–400 m) BPE. SST indices, APE, BPE and wind stress values were calculated using SODA data and have been detrended.

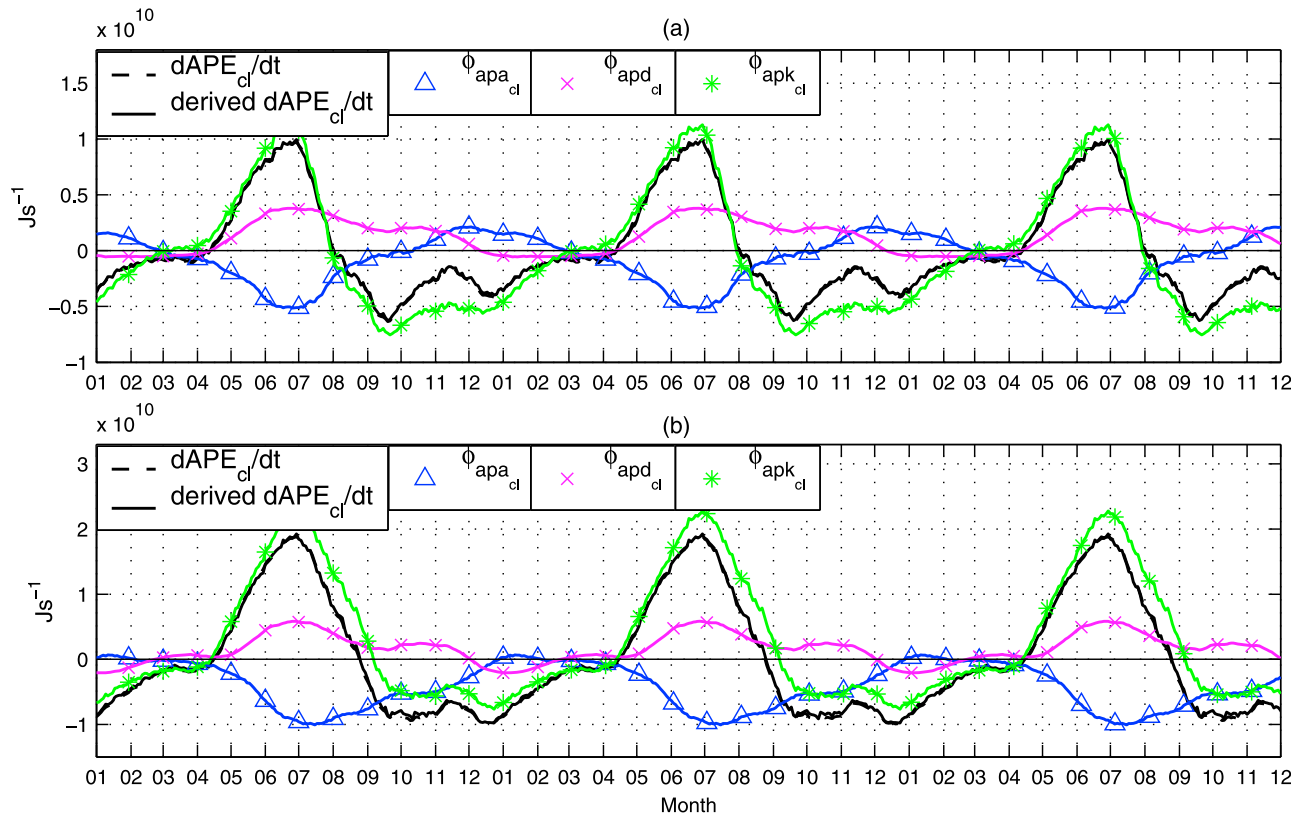


Figure 3. The climatological balance of terms (Js^{-1}) for the APE evolution equation, assessed over (a) the equatorial Atlantic domain (3°S – 3°N 60°W – 15°E 0 – 400 m), and (b) the tropical Atlantic domain (8°S – 8°N 60°W – 15°E 0 – 400 m). Following equation (A1), $\Phi_{apk_{cl}}$ represents the buoyancy power term, $\Phi_{apa_{cl}}$ the advection of local APE across the surfaces of the volume and $\Phi_{apd_{cl}}$ the combined effects of changes in PE due to mixing within the domain, the rate of change of BPE driven by diapycnal mixing, and changes in APE due to the surface buoyancy flux. A 14 day running mean has been applied to the time series to smooth out the high frequency variability.

APE changes in the Pacific to be the buoyancy power term. Representing the vertical motion of the mass field, buoyancy power creates thermocline perturbations. The approximation that equatorial/tropical basin APE changes are driven primarily by buoyancy forcing associated with the horizontal redistribution of warm surface waters is therefore seen to hold when evaluating seasonal APE changes in the Atlantic having taken into account seasonal changes in BPE (equation (6))

$$\frac{dAPE_{cl}}{dt} \approx \underbrace{\int \int \int g \tilde{\rho}_{cl} w_{cl} dV}_{\Phi_{apk_{cl}}}. \quad (6)$$

[37] The buoyancy power term is the reversible exchange term between the APE and KE evolution equations and so further insight can be gained into the processes responsible for buoyancy power fluctuations by considering the KE evolution equation (equation (A2)). Figure 4 shows the full climatological balance of terms for the KE evolution equation (equation (A2)) assessed over the equatorial Atlantic domain and the tropical Atlantic domain respectively. In both domains, the wind power term ($\Phi_{ww_{cl}}$) is the dominant source term. Only a portion of the wind power is converted into buoyancy power ($\Phi_{apk_{cl}}$). As in the Pacific [Goddard

and Philander, 2000; Fedorov, 2007; Brown and Fedorov, 2010], a small percentage of the work done on the ocean by the wind translates into KE changes (dKE/dt). A large portion of the wind power is dissipated and the residual forces buoyancy power fluctuations. The dissipation of work done by the wind is seen in both domains to be primarily due to shear stresses of horizontal flows within each domain ($\Phi_{ss_{cl}}$) with the advection of KE out of each domain ($\Phi_{ka_{cl}}$) playing a smaller dissipative role. The pressure work term ($\Phi_{pw_{cl}}$) representing the work done against internal and surface pressure gradients by ageostrophic flow is found to dissipate the work done by the wind during certain months of the year. This term changes sign from an energy sink to an energy source term seasonally, however its seasonal fluctuations are significantly less than that of the primary source term, namely wind power and the primary dissipative term, namely the dissipation due to shear stresses of horizontal flows.

[38] One would expect the horizontal redistribution of warm surface waters, which gives rise to seasonal buoyancy power and hence seasonal APE changes in the Atlantic, to be primarily related to fluctuations in the primary source term, namely wind power over the domain. In Figure 5, seasonal fluctuations in the buoyancy power term are compared with seasonal fluctuations in the wind power term

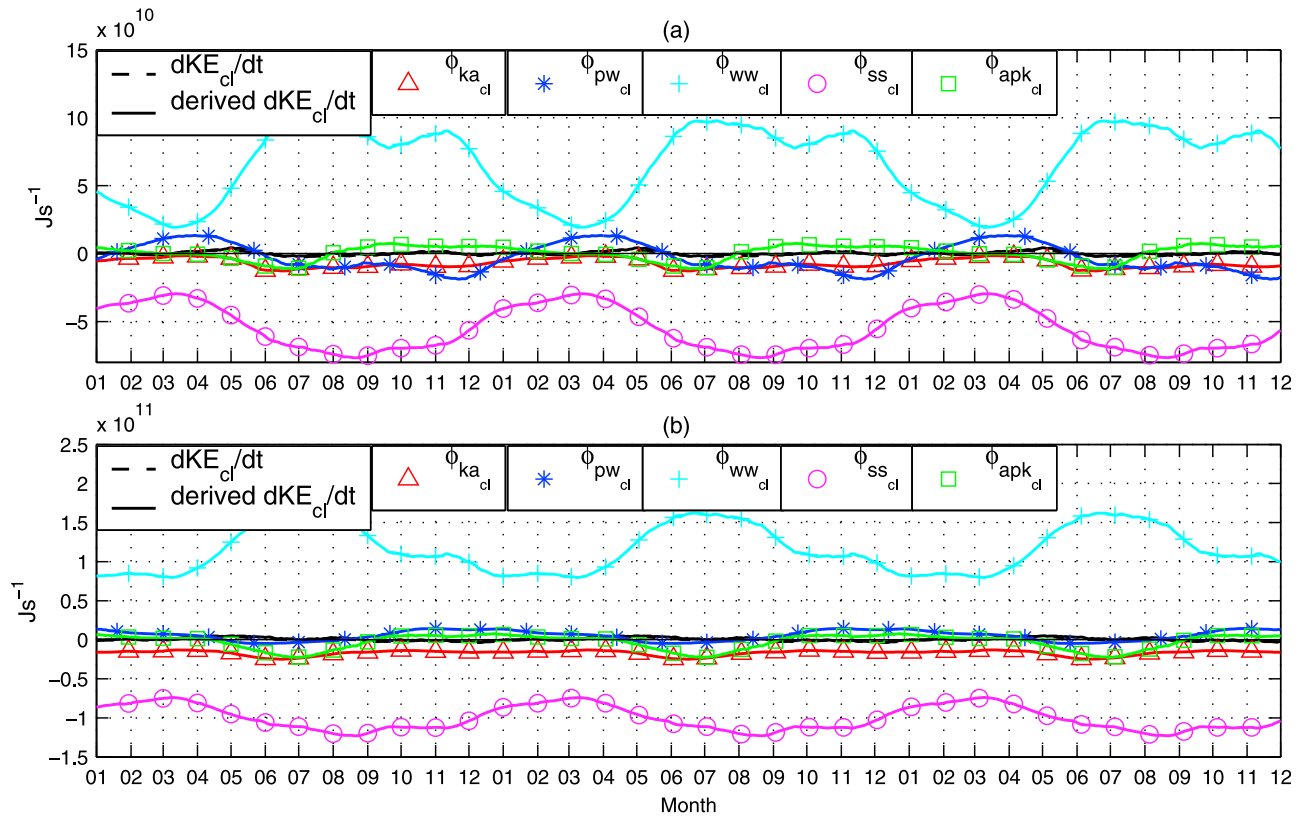


Figure 4. The climatological balance of terms (Js^{-1}) for the KE evolution equation, assessed over (a) the equatorial Atlantic domain (3°S – 3°N 60°W – 15°E 0 – 400 m), and (b) the tropical Atlantic domain (8°S – 8°N 60°W – 15°E 0 – 400 m). Following equation (A2), $\Phi_{ka_{cl}}$ represents the advection of KE across the surfaces of the volume, $\Phi_{pw_{cl}}$ the pressure work across the surfaces of the volume, $\Phi_{apk_{cl}}$ the buoyancy power term, $\Phi_{ww_{cl}}$ the work done by the wind stress acting on surface currents and $\Phi_{ss_{cl}}$ the work done by shear stresses of horizontal flows within the domain. A 14 day running mean has been applied to the time series to smooth out the high frequency variability. Note $\Phi_{apk_{cl}}$ values in this KE evolution equation balance are the inverse of $\Phi_{apk_{cl}}$ values given for the APE evolution equation (Figure 3).

for both the equatorial and tropical Atlantic domains. In Figure 5b, seasonal changes in the buoyancy power within the tropical Atlantic domain follow seasonal changes in the work done by the wind over this domain. This relationship is not observed however for the equatorial domain (Figure 5a), as wind power and seasonal buoyancy power changes are not totally in-phase. This difference is attributed to the larger influence of processes acting at the meridional boundaries of the equatorial domain than at the meridional boundaries of the tropical domain. For the equatorial domain both physical processes operating within the domain ($\Phi_{ww_{cl}}$ and $\Phi_{ss_{cl}}$) and processes acting at the boundaries ($\Phi_{pw_{cl}}$ and $\Phi_{ka_{cl}}$) appear to play a significant role in driving seasonal buoyancy power changes [Burls, 2010]. Seasonal APE changes within the equatorial domain are therefore driven not only by seasonal changes in the work done by the wind within the equatorial domain but also by the response of the greater tropical Atlantic domain to seasonal fluctuations in wind forcing via its impact along the meridional boundaries of the equatorial domain. As seen interannually in the Pacific [Goddard and Philander, 2000], the larger influence of processes acting at the meridional boundaries of the equatorial domain, points to the significant contribution of off-equatorial adjustment on buoyancy power within the equatorial domain, as sea-

sonally excited transients enter and exit the equatorial domain. This finding is consistent with conclusions drawn in previous studies that eastern and western boundary reflections play an important role in seasonal equatorial SSH variability [Philander and Pacanowski, 1986a; Schouten et al., 2005; Ding et al., 2009] and that the contribution of Kelvin and Rossby waves reflected at these boundaries to simulated equatorial SSH variability is equal to directly forced waves [Ding et al., 2009]. The fact that off-equatorial adjustment and boundary reflections play an important role in driving equatorial variability reinforces the suggestion that the Bjerknes feedback and delayed, ocean memory, negative feedback are seasonally active in the Atlantic.

[39] Extending the domain over which APE is evaluated to include the tropical domain reduces the dominant processes governing seasonal APE variability down to one dominant process, namely seasonal fluctuations in the work done by the wind over the tropical Atlantic domain ($\Phi_{ww_{cl}} = \int_{z=0} \mathbf{v}_{cl} \cdot \boldsymbol{\tau}_{s_{cl}} dS = \int_{z=0} u_{cl} \tau_{s_{cl}}^x + v_{cl} \tau_{s_{cl}}^y dS$). The meridional extent of the tropical domain chosen here, 8°S – 8°N , is deemed large enough to encompass the wind forced region over which seasonal buoyancy power changes are predominantly related to wind power fluctuations, yet small enough

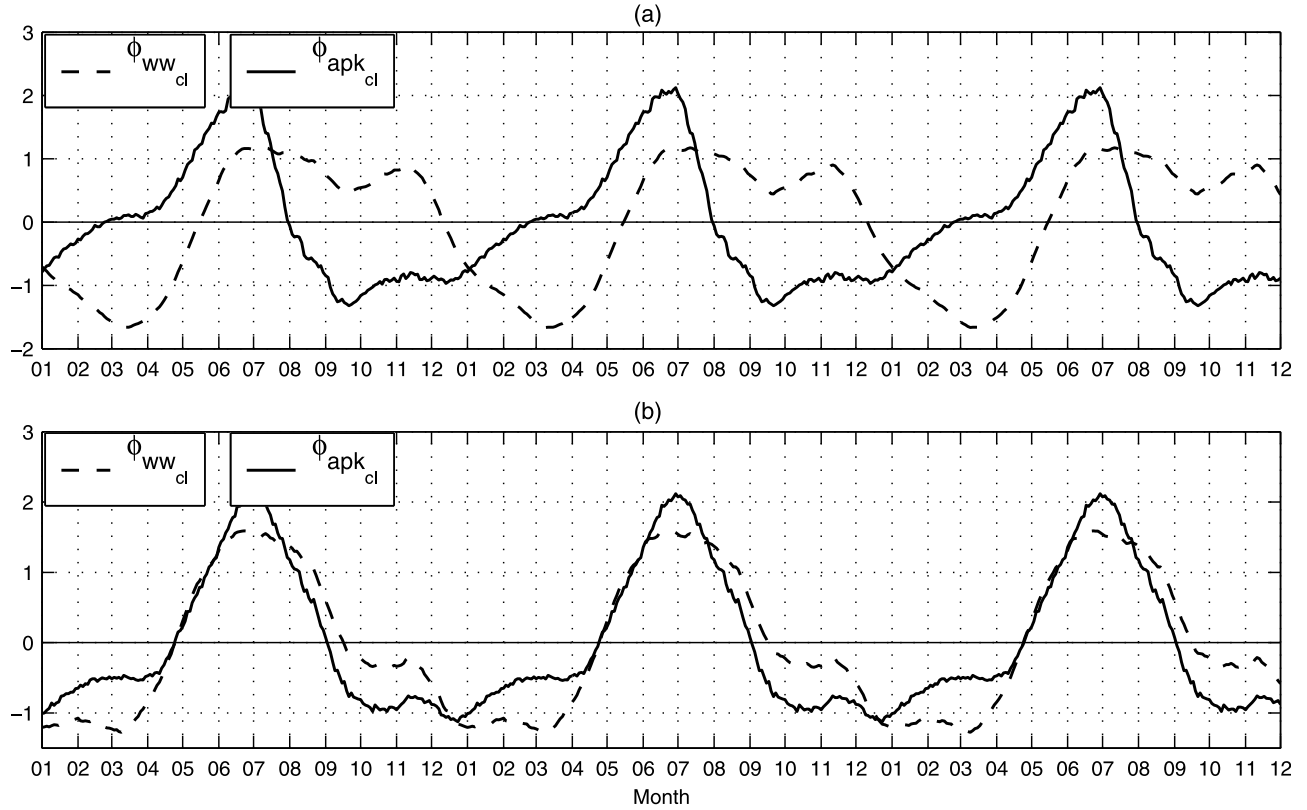


Figure 5. A comparison between seasonal fluctuations in buoyancy power ($\Phi_{apk_{cl}}$) and wind power ($\Phi_{ww_{cl}}$) for (a) the equatorial Atlantic domain (3°S–3°N 60°W–15°E 0–400 m), and (b) the tropical Atlantic domain (8°S–8°N 60°W–15°E 0–400 m). Buoyancy power ($\Phi_{apk_{cl}}$) and wind power ($\Phi_{ww_{cl}}$) values have been normalized. A 14 day running mean has been applied to the time series to smooth out the high frequency variability.

to preserve the strong relationship with At13 SST and limit the lag-lead in this relationship.

[40] The relative contribution of the zonal ($\Phi_{ww_{cl}}^x = \int \int_{z=0} u_{cl} \tau_{s_{cl}}^x dS$) and meridional ($\Phi_{ww_{cl}}^y = \int \int_{z=0} v_{cl} \tau_{s_{cl}}^y dS$) components of the wind power term to climatological wind power values has been examined (not shown, see *Burls* [2010]). Zonal wind stress acting on zonal surface currents is clearly responsible for the majority of work done on the ocean by the wind within the tropical Atlantic $\Phi_{ww_{cl}} \approx \Phi_{ww_{cl}}^x$. Making the assumption that seasonal wind power fluctuation may be approximated by the work done by zonal winds acting on zonal surface currents, $\Phi_{ww_{cl}} \approx \Phi_{ww_{cl}}^x$, this term is decomposed into its mean, $\Phi_{ww_{cl}}^{mm} = \int \int_{z=0} \overline{u_{cl} \tau_{s_{cl}}^x} dS$, mean perturbation, $\Phi_{ww_{cl}}^{mp} = \int \int_{z=0} u'_{cl} \overline{\tau_{s_{cl}}^x} dS + \int \int_{z=0} \overline{u_{cl}} \tau'_{s_{cl}} dS$, and perturbation, $\Phi_{ww_{cl}}^{pp} = \int \int_{z=0} u'_{cl} \tau'_{s_{cl}} dS$ components

$$\begin{aligned}
 \Phi_{ww_{cl}}^x &= \int \int_{z=0} u_{cl} \tau_{s_{cl}}^x dS \\
 &= \int \int_{z=0} (\overline{u_{cl}} + u'_{cl}) (\overline{\tau_{s_{cl}}^x} + \tau'_{s_{cl}}) dS \\
 &= \underbrace{\int \int_{z=0} \overline{u_{cl}} \overline{\tau_{s_{cl}}^x} dS}_{\Phi_{ww_{cl}}^{mm}} + \underbrace{\int \int_{z=0} u'_{cl} \overline{\tau_{s_{cl}}^x} dS + \int \int_{z=0} \overline{u_{cl}} \tau'_{s_{cl}} dS}_{\Phi_{ww_{cl}}^{mp}} \\
 &\quad + \underbrace{\int \int_{z=0} u'_{cl} \tau'_{s_{cl}} dS}_{\Phi_{ww_{cl}}^{pp}}.
 \end{aligned} \tag{7}$$

[41] This decomposition is similar to that done by *Goddard and Philander* [2000] except that they evaluated the effect of interannual zonal wind stress and zonal current perturbations from climatological values. In this context, $\overline{\tau_{s_{cl}}^x}$ and $\overline{u_{cl}}$ represent mean zonal wind stress and surface current values, while $\tau'_{s_{cl}}$ and u'_{cl} represent seasonal perturbations from these mean fields. The mean perturbation component of wind power, $\Phi_{ww_{cl}}^{mp}$, comprises of two terms - $\Phi_{ww_{cl}}^{mp\tau} = \int \int_{z=0} \overline{u_{cl}} \tau'_{s_{cl}} dS$, which represents the effect of seasonal zonal wind stress fluctuations on mean surface currents and $\Phi_{ww_{cl}}^{mpu} = \int \int_{z=0} u'_{cl} \overline{\tau_{s_{cl}}^x} dS$, representing the effect of the mean wind field acting on seasonal surface current variations associated with the adjustment of the ocean. In Figure 6, the relative contribution of mean perturbation terms $\Phi_{ww_{cl}}^{mp\tau}$ and $\Phi_{ww_{cl}}^{mpu}$ as well as the perturbation term, $\Phi_{ww_{cl}}^{pp}$, to seasonal fluctuation in zonal wind power, $\Phi_{ww_{cl}}^x - \Phi_{ww_{cl}}^{mm}$, is assessed. Seasonal fluctuations in wind power are seen to be predominantly driven by the mean perturbation terms, $\Phi_{ww_{cl}}^{mp\tau}$ and $\Phi_{ww_{cl}}^{mpu}$.

[42] Figure 7 compares seasonal changes in the magnitude of the mean perturbation term, $\Phi_{ww_{cl}}^{mp\tau}$, with seasonal fluctuations in zonal wind stress integrated over the tropical Atlantic domain (8°S–8°N 60°W–15°E) and wind stress integrated over the region in which the mean zonal surface velocity field has the strongest westward values (8°S–2°N 50°W–0°E). Evident in Figure 7 is that the domain integrated seasonal zonal wind stress fluctuations differ

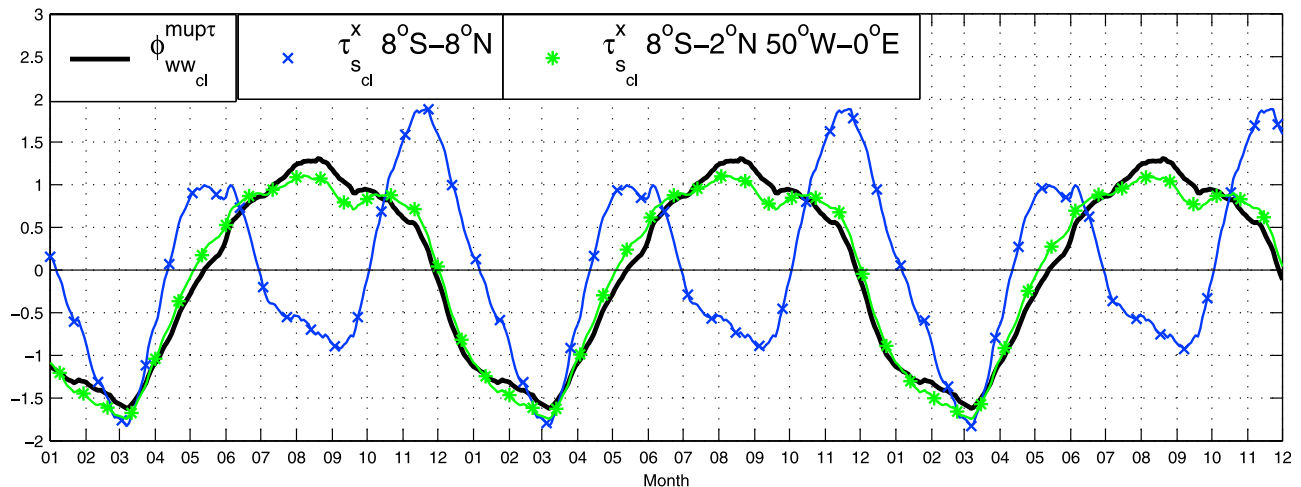


Figure 7. A comparison between seasonal fluctuations in the mean perturbation term, $\Phi_{ww,cl}^{mupt}$, seasonal fluctuations in zonal wind stress integrated over the tropical Atlantic domain ($8^{\circ}\text{S}–8^{\circ}\text{N}$ $60^{\circ}\text{W}–15^{\circ}\text{E}$), and seasonal fluctuations in zonal wind stress integrated over $8^{\circ}\text{S}–2^{\circ}\text{N}$ $50^{\circ}\text{W}–0^{\circ}\text{E}$. Values have been normalized. A 14 day running mean has been applied to the time series to smooth out the high frequency variability.

(Figure 6) likewise corresponds to an increase in wind power within this region (Figures 8k and 8l).

[45] As shown at the beginning of this section, the dominant source of seasonal buoyancy power fluctuations for the tropical Atlantic are seasonal fluctuations in the wind power term (Figure 5b). Seasonal fluctuations in the wind power term are converted into seasonal APE changes via the buoyancy term (Figure 3b). Figure 9 shows the spatial structure and temporal evolution of climatological, vertically integrated, buoyancy power perturbations from the annual mean over the tropical Atlantic. As seen in Figures 8a–8c tropical Atlantic wind power values are relatively low between January and March. As a result, vertically integrated buoyancy power perturbations from the annual mean are negative over most of the tropical Atlantic during these months (Figures 9a–9c). Increased wind power during May, June and July (Figures 8e–8g) results in positive buoyancy power perturbations in the eastern equatorial Atlantic and off the coast of southern Africa as transient oceanic adjustment shoals the thermocline in these regions (Figures 9e–9g). Positive buoyancy power perturbations are also seen in the western tropical Atlantic as downwelling off-equatorial Rossby waves deepen the thermocline in this region. Linked with the westward propagation and decreased extent of positive seasonal wind power values between July and October (Figures 8g–8j) are negative buoyancy power values along the equatorial wave guide and coast of southern Africa as both of these features are associated with the delayed, ocean memory, negative feedback discussed further in section 3.3.

[46] The results obtained within this section show that the annual increase in zonal wind forcing between $8^{\circ}\text{S}–2^{\circ}\text{N}$ $50^{\circ}\text{W}–0^{\circ}\text{E}$ is responsible for the rapid seasonal increase in equatorial Atlantic APE between April and August, therefore providing evidence that the second element of the Bjerknes feedback plays an active role in the development of the cold tongue.

3.2.2. The Role of Remotely Forced Heat Content Changes Within Seasonal Central-Eastern Basin SST Variability

[47] Seasonal Atl3 SST changes are highly anti-correlated with the large seasonal changes seen in equatorial Atlantic APE, as depicted in Figure 10 which illustrates the relationship between seasonal Atl3 SST changes and equatorial Atlantic APE changes ($r = -0.97$, $r^* = -0.67$). This strong relationship between large fluctuations in APE and central-eastern Atlantic SST implies that remotely forced thermocline depth variability, a process which only plays a significant role interannually in the Pacific, plays a key role in regulating subsurface cooling and hence seasonal SST variability in the Atlantic. Previous studies have shown that seasonal SST fluctuations in the central-eastern equatorial Atlantic are regulated primarily by warming, due to the surface heat flux and oceanic eddies, and subsurface cooling [Weingartner and Weisberg, 1991; Carton and Zhou, 1997; Foltz et al., 2003; Peter et al., 2006]. In this section, surface layer heat budgets for the Atl3 region have been conducted (based on the ROMS-TAtl simulation as outlined in section 2.3). The goal is to facilitate a comparison with not only previous results but also the energetics of the equatorial Atlantic in an attempt to establish the role of remotely forced ocean dynamics within seasonal central-eastern equatorial Atlantic SST variability.

[48] Seasonal variations in the temperature of the SML and SST for the Atl3 region are compared in Figure 11a. Seasonal variations in the mean temperature of the SML correspond closely to seasonal SST changes (Figure 11a). As shown in Figure 11b, the dominant terms forcing these seasonal changes are the surface heat flux and vertical mixing. The horizontal advection terms play a secondary but still significant role, while contributions from the vertical advection, horizontal mixing and entrainment are minimal. Simulated vertical velocities at the base of the SML are weak as turbulent processes dominate, hence vertical advection is a small term and subsurface cooling takes the

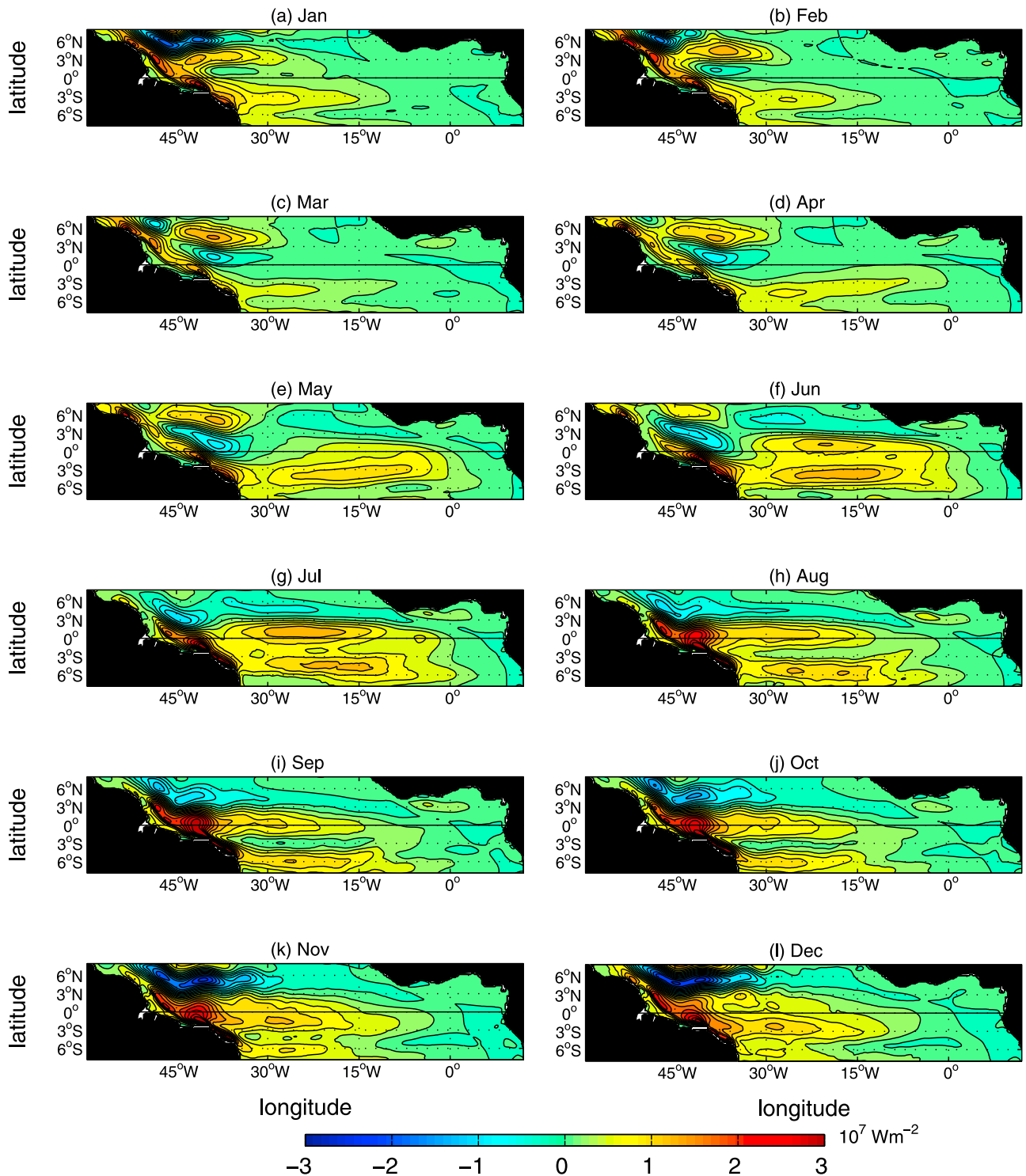


Figure 8. Monthly maps illustrating the spatial structure in the climatological wind power flux (Wm^{-2}) over the tropical Atlantic.

form of vertical mixing at this depth. As discussed by *Menkes et al.* [2006], the negligible effect of entrainment is due to the distinction between the mixed layer (defined following criteria on tracers) and the mixing layer (defined from the vertical mixing coefficient) depths [*Brainerd and Gregg, 1995*].

[49] The dominant term forcing seasonal changes in the mean temperature of the WWL is vertical advection (Figure 11c), followed by the horizontal advection terms and surface heating. Contributions from the mixing terms are minimal. Seasonal fluctuations in the mean temperature of the WWL layer mirror seasonal SST changes (Figure 11a) particularly between April and September. As shown below

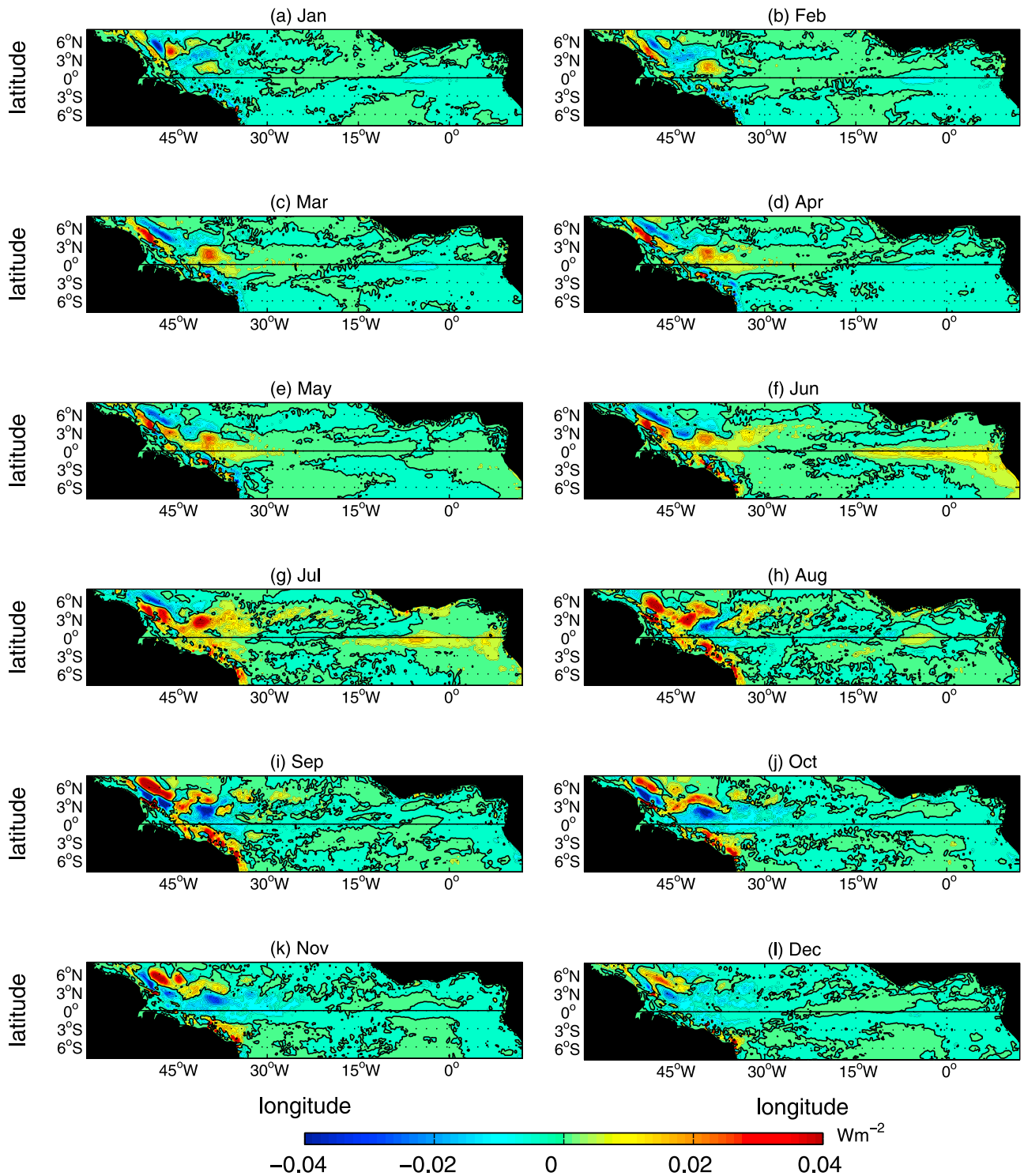


Figure 9. Monthly maps illustrating the spatial structure of climatological, vertically integrated, buoyancy power perturbations from the annual mean (Wm^{-2}) over the tropical Atlantic.

this covariability is due to the fact that enhanced vertical mixing at the base of the SML couples the subsurface with the surface during these months (Figure 11b). Seasonal fluctuations in the mean temperature of these two layers do not correspond as well between October and March (Figure 11a), as surface heating warms the SML, increasing

stratification, reducing mixing at the base of the mixed layer (Figure 11b), and decoupling it from the subsurface.

[50] For both the SML and WWL seasonal heat budgets (Figures 11b and 11c), a sharp increase in the intensity of subsurface cooling is seen to be responsible for the rapid April-August temperature change. This subsurface cooling takes the form of enhanced vertical mixing for the SML and

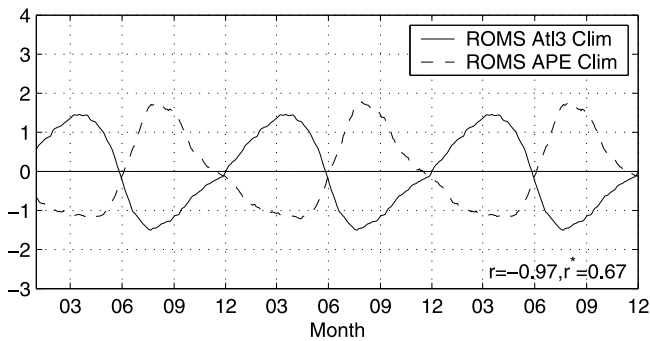


Figure 10. A comparison between climatological At13 (3°S – 3°N 20°W – 0°E) SST and equatorial Atlantic (3°S – 3°N 60°W – 15°E 0 – 400 m) APE. The correlation between the At13 SST index and equatorial Atlantic APE values (r) is given, together with the required correlation value for significance at the 95% level taking into account the effective degrees of freedom (r^*). SST and APE values were calculated using ROMS-TAtl data and have been normalized.

vertical advection for the WWL. The magnitude of SML cooling due to simulated vertical mixing at the base of the SML (term V in equation (5)) is controlled by seasonal changes in three variables: (1) the vertical temperature gradient at the base of the mixed layer, (2) the strength of the vertical temperature diffusion coefficient at the base of the mixed layer and (3) the depth of the SML. Figure 12 shows the seasonal variability within these variables for the At13 region. Figure 12a illustrates the seasonal variations in the vertical temperature gradient and temperature diffusion coefficient at the depth of the SML, while Figures 12b and 12c illustrate the vertical context in which these changes are taking place. As shown in Figures 12a and 12b, vertical temperature gradient changes at the base of the mixed layer appear to play the most important role in the May–July increase, and August–October decrease, of vertical mixing at the base of the SML (Figure 11b). The seasonal increase in the vertical temperature diffusion coefficient at the base of the mixed layer peaks later (Figure 12a) and is counteracted by an increase in the SML depth (Figure 12c) as the intensity of cooling due to vertical mixing at the base of the SML (term V in equation (5)) peaks in June/July (Figure 11b). According to this model based analysis, the vertical temperature diffusion coefficient at the base of the SML (determined following the non-local, K-Profile Planetary (KPP) boundary layer scheme of *Large et al.* [1994]) is at a maximum in September/October. As resolved by the surface layer heat budget for the deeper WWL (Figure 11c), the temperature of water at the base of the SML that is mixed into the SML is largely determined by vertical advection acting below the depth of the SML (Figure 12b). Evident in Figures 12a and 12b, enhanced cooling due to vertical advection (upwelling) acts to decrease the temperature at the base of the SML and is responsible for the increase in the vertical temperature gradient at the base of the SML between April and June.

[51] Having established that subsurface temperature variations, driven by fluctuations in vertical advection at the base of the WWL, are reflected in the SST field by vertical mixing at the base of the SML, the focus shifts to the

processes driving the seasonal changes in vertical temperature advection at the base of the WWL. Changes in the magnitude of vertical temperature advection may result from either locally forced changes in vertical Ekman velocities or remotely forced thermocline depth changes. The in-phase relationship between seasonal APE and At13 SST fluctuations seen in Figure 10 suggests that the large annual increase in the intensity of cooling due to vertical advection is not purely a locally forced phenomena, but largely due to the horizontal redistribution of warm surface waters in response to large scale changes in wind forcing. The seasonal shoaling of the thermocline in the east as APE increases is clearly visible in observed climatological temperature fields along the equator (Figure 13). Figure 13 compares simulated values with monthly climatological temperature profiles derived from PIRATA mooring data [*Servain et al.*, 1998] at three sites along the equator $0^{\circ}\text{N}35^{\circ}\text{W}$, $0^{\circ}\text{N}10^{\circ}\text{W}$ and $0^{\circ}\text{N}0^{\circ}\text{E}$. The ROMS-TAtl simulation reproduces the seasonal variations observed in the vertical temperature structure well, although the thermocline is seen to be slightly more diffuse than in reality. One can compare Figure 13 with a similar figure created for the Pacific, Figure 9 of *McPhaden et al.* [1998], in which the thermocline hardly varies seasonally.

[52] Figure 14 has been created to diagnose the relative contribution of local Ekman pumping versus remotely forced changes in the vertical temperature structure (quantified using equatorial APE values) to the seasonal increase in vertical advection associated with the development of the cold tongue. Figure 14 compares seasonal variations in the magnitude of the vertical temperature advection term for the At13 WWL (term A_z in equation (5) and Figure 11c) with seasonal variations in Ekman pumping velocities and the rate of change of equatorial Atlantic APE (note that vertical temperature advection values have been inverted in Figure 14 to facilitate the comparison). Clearly illustrated by Figure 14 is the fact that increased cooling due to vertical advection coincides with the forcing of equatorial Atlantic APE changes rather than locally enhanced vertical velocities due to Ekman pumping. This points to the importance of remotely forced changes in the horizontal distribution of warm surface waters in the annual development of the equatorial Atlantic cold tongue.

[53] As a surface expression of large seasonal change in the subsurface temperature structure of the eastern equatorial Atlantic, At13 SST reaches an annual minimum during July–August as APE values in the eastern equatorial Atlantic peak (Figure 10). In August the shoaling of the thermocline in the east slows and it begins to deepen during September and October (Figure 13). APE values decrease during this period (Figure 10), local upwelling velocities weaken (Figure 14) and subsurface cooling of the WWL driven by vertical advection decreases (Figure 11c). This decreased vertical advection is associated with a decrease in the vertical temperature gradient at the base of the mixed layer (Figures 12a and 12b) and hence a decrease in subsurface cooling of the SML driven by vertical mixing. SST in the central-eastern basin increases during September and October as decreased subsurface cooling together with increased solar heating raise the heat storage of the SML (Figure 11) [*Peter et al.*, 2006].

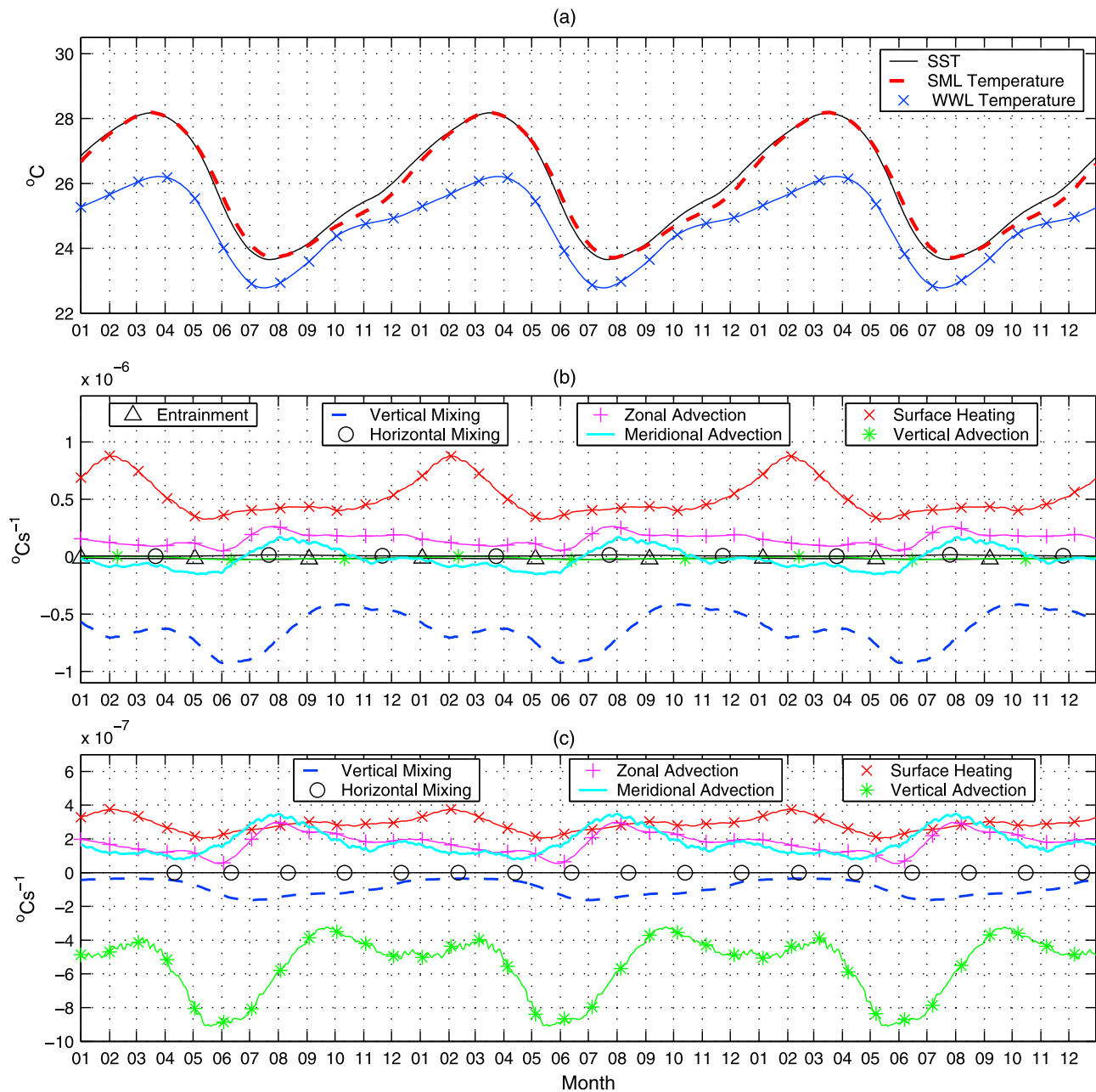


Figure 11. (a) Seasonal variations in SST, the average temperature of the Surface Mixed Layer (SML) (varying depth), and the average temperature of the Warm Water Layer (WWL) (fixed depth = 70 m) for the Atl3 region. Climatology of terms contributing to seasonal variations in the mean temperature of (b) the SML, and (c) the WWL. A 14 day running mean has been applied to the time series to smooth out the high frequency variability.

[54] In the central-eastern Atlantic, the zonal component of the trades intensifies slightly in November/December abating the decrease in vertical Ekman velocities for the Atl3 region (Figure 14). The thermocline is also seen to shoal slightly (Figure 13). This shoaling of the thermocline is reflected in the APE signal (Figure 10) as the decrease in equatorial APE slows during these months. In the Atl3 SST index, only the rate of increase in Atl3 SST is seen to decrease during this period (Figure 11), as this somewhat weaker second cooling event during the months of November-December is confined to a small near-equatorial region within

the central-eastern equatorial Atlantic [Okumura and Xie, 2006] and is therefore less evident within this analysis over the large Atl3 region.

[55] The symmetrical latitudinal extent of the Atl3 region each side of the equator isolates east-west effects, masking the asymmetries that result from the significant meridional component in the wind stress. These equatorial asymmetries can be seen when dividing the Atl3 region into a southern Atl3 region (0°N – 3°S 60°W – 15°E) and northern Atl3 region (3°N – 0°S 60°W – 15°E) (not shown, see Burls [2010]). While the signature of seasonal SST changes are similar, Atl3 SST

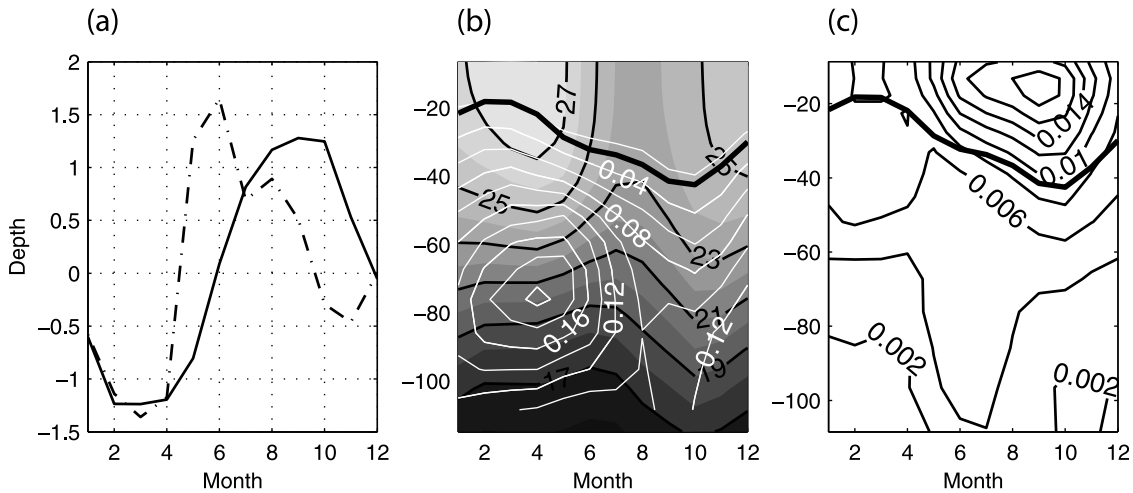


Figure 12. (a) Seasonal changes in the vertical temperature gradient (dashed line) and the vertical temperature diffusion coefficient (solid line) at the base of the Surface Mixed Layer for the Atl3 region (values have been normalized to facilitated a comparison). (b) Seasonal changes in the SML depth (thick black contour), temperature (shading over-layered with black contours in $^{\circ}\text{C}$) and the vertical temperature gradient (white contours in $^{\circ}\text{Cm}^{-1}$), for the Atl3 region. (c) Seasonal changes in the SML depth (thick black contour) and the vertical temperature diffusion coefficient (black contours in m^2s^{-1}) for the Atl3 region.

north of the equator is significantly warmer and seasonal changes south of the equator are seen to lead slightly those north of the equator. The southerly cross-equatorial component in winds over the Atl3 region drives positive Ekman vertical velocities south of the equator and negative velocities north of the equator throughout the year. Despite very similar seasonal cycles in the rate of change of SML temperature for the northern and southern Atl3 regions, the dominant terms forcing these temperature rates are somewhat different. In the south, the signature of seasonal fluctuation is attributable mainly to fluctuations in vertical mixing and surface heating (not shown, see *Burls* [2010]). In the northern Atl3 region, the horizontal advection terms are comparable in magnitude to the vertical mixing and surface heating terms, becoming an important element in driving seasonal SML temperature changes.

[56] The results obtained within this section show that seasonal thermocline depth fluctuations in the central-eastern equatorial Atlantic translate into SST fluctuations therefore providing evidence that the third element of the Bjerknes feedback is seasonally active. Overall, the findings presented in this section (section 3.2) point to the fact Bjerknes feedback is seasonally excited in April/May, resulting in the steep seasonal increase in equatorial Atlantic APE and associated decline in central-eastern basin SST as the Atlantic cold tongue develops.

3.3. The Seasonally Active Delayed Negative Feedback Mechanism

[57] The analysis of the ROMS-TAtl simulation performed in this section is aimed at establishing the mechanism associated with the decay of the seasonally excited

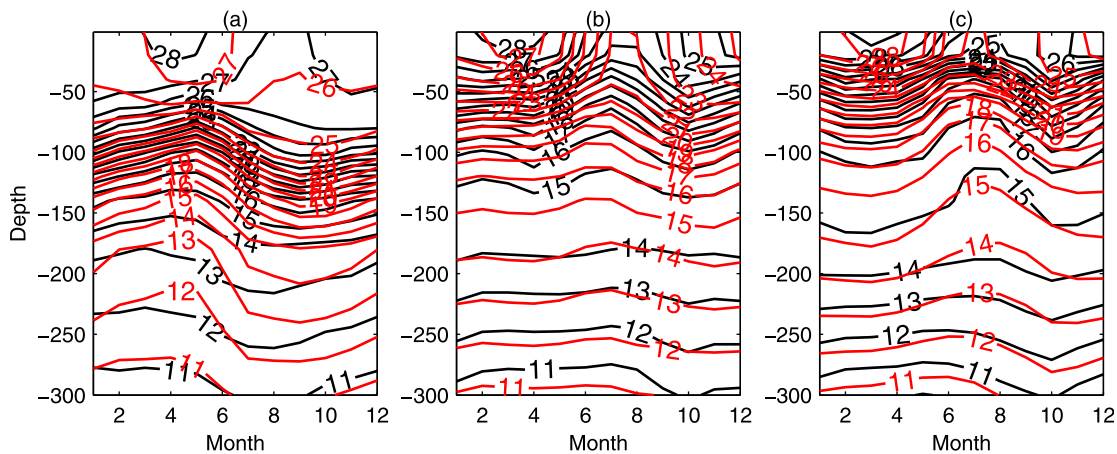


Figure 13. A monthly climatology of temperature profiles in $^{\circ}\text{C}$ for three sites on the equator (a) 0°N , 35°W , (b) 0°N , 10°W and (c) 0°N , 0°E . (Black contours) climatology derived from PIRATA mooring data [*Servain et al.*, 1998]. (Red contours) climatology derived from ROMS-TAtl simulation.

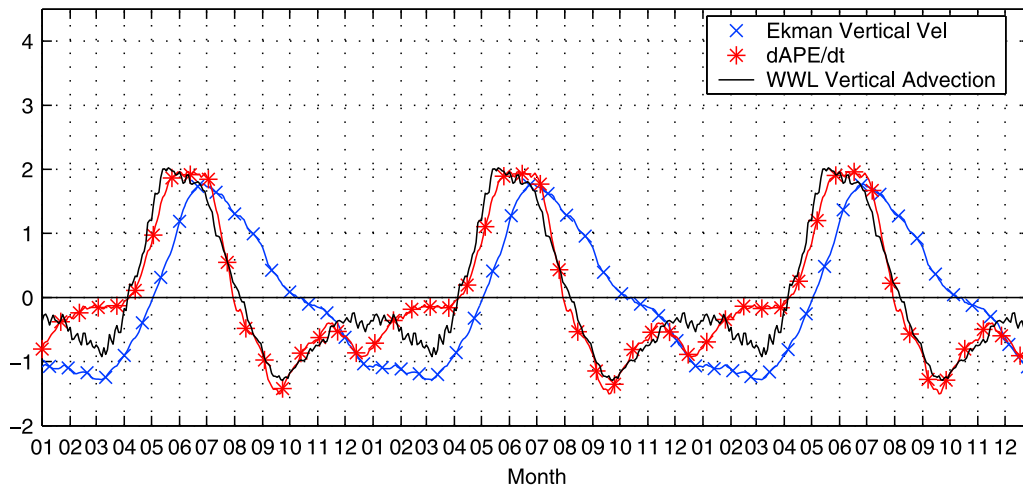


Figure 14. Seasonal variations in the intensity of the vertical temperature advection term for the Atl3 Warm Water Layer (WWL) heat budget are compared with seasonal variations in Ekman vertical velocities for the Atl3 region and the rate of change of equatorial Atlantic (3°S – 3°N 60°W – 15°E 0 – 400 m) APE. Note that, vertical temperature advection values have been inverted to facilitate the comparison. Ekman vertical velocities, APE rate of change and vertical advection values have been normalized. A 14 day running mean has been applied to the time series to smooth out the high frequency variability.

Bjerknes feedback. As shown in section 3.2.2 (Figure 11), a decrease in subsurface cooling is responsible for the warming in Atl3 SST seen between August and October. In accordance with a delayed, ocean memory, negative feedback mechanism this decrease in subsurface cooling is linked with a deepening of the thermocline in the central-eastern equatorial Atlantic and a decrease in APE (Figures 10 and 13).

[58] Regarding this warming as the surface expression of the associated decrease in upper ocean APE, the processes responsible for the August–October increase in Atl3 SST can be established by investigating the processes responsible for the decrease in APE. As shown in section 3.2.1 equatorial/tropical basin APE changes are driven primarily by the buoyancy power term (Figure 3). In Figures 8h–8j we see that domain integrated negative buoyancy power values, force the decrease in equatorial APE from August (Figure 3a), are due to negative buoyancy power values along the equatorial wave guide and off the coast of southern Africa. These negative buoyancy power values are attributed to downwelling Kelvin waves caused by the reflection of downwelling off-equatorial Rossby waves excited between April and June. The sudden onset of enhanced zonal wind stress forcing east of 30°W in May occurs at a much shorter timescale than the adjustment timescale of the equatorial Atlantic [Philander and Pacanowski, 1986a]. This sudden intensification is seen to excite upwelling equatorial Kelvin waves and downwelling off-equatorial Rossby waves [Schouten et al., 2005; Ding et al., 2009] (Figures 9e–9g). The upwelling equatorial Kelvin waves and downwelling off-equatorial Rossby waves are then reflected at the eastern and western boundaries respectively [Ding et al., 2009]. Unlike the Pacific [Yu and McPhaden, 1999], boundary (coastal) reflections are seen to play an important role in seasonal SSH variability in the tropical Atlantic [Philander and Pacanowski, 1986a; Schouten et al., 2005; Ding et al., 2009].

[59] The effect of this oceanic adjustment is seen in the wind power term - the source of buoyancy power fluctuations (Figure 5b). Kelvin and Rossby wave propagation results in an acceleration of westward surface flow between April–June followed by a deceleration of westward surface flow between July–October and then a subsequent acceleration in November–December [Philander and Pacanowski, 1986a; Schouten et al., 2005; Ding et al., 2009]. The influence of these seasonal surface current changes on the ability of the wind to do work on the tropical ocean is resolved by term $\Phi_{ww,el}^{m\tau pu}$. As indicated by the dashed arrows in Figure 6, this term peaks at the end of May and reaches a minimum at the end of September. A secondary peak smaller peak is also seen in December.

[60] The sensitivity experiments of Biasutti et al. [2005] and Li and Philander [1997] suggest that seasonal variations in land temperature and precipitation, forced by the annual cycle in insolation over the surrounding continents, play an equally important role as seasonal changes in oceanic insolation and dynamic oceanic processes in the annual migration of the ITCZ and associated wind changes - particularly with respect to the southward migration of the ITCZ in boreal spring. Whether forced by seasonal variations in tropical Atlantic SST or atmospheric convection over the surrounding continents, the effect of seasonal tropical Atlantic surface wind changes is captured in term $\Phi_{ww,el}^{m\tau pu}$ (Figure 6). As seen in Figure 6, this term is not responsible for the decline in wind power over the tropical Atlantic from late June, as enhanced zonal wind stress in the western Atlantic continues to increase term $\Phi_{ww,el}^{m\tau pu}$ up until the end of August. The reason why this enhanced wind stress does not continue to increase wind power over the tropical Atlantic is because surface current deceleration effects the ability of seasonal zonal wind stress changes to do work on the ocean as captured by term $\Phi_{ww,el}^{m\tau pu}$ in Figure 6.

[61] Figure 15 shows the spatial structure and temporal evolution of the zonal surface current variability associated

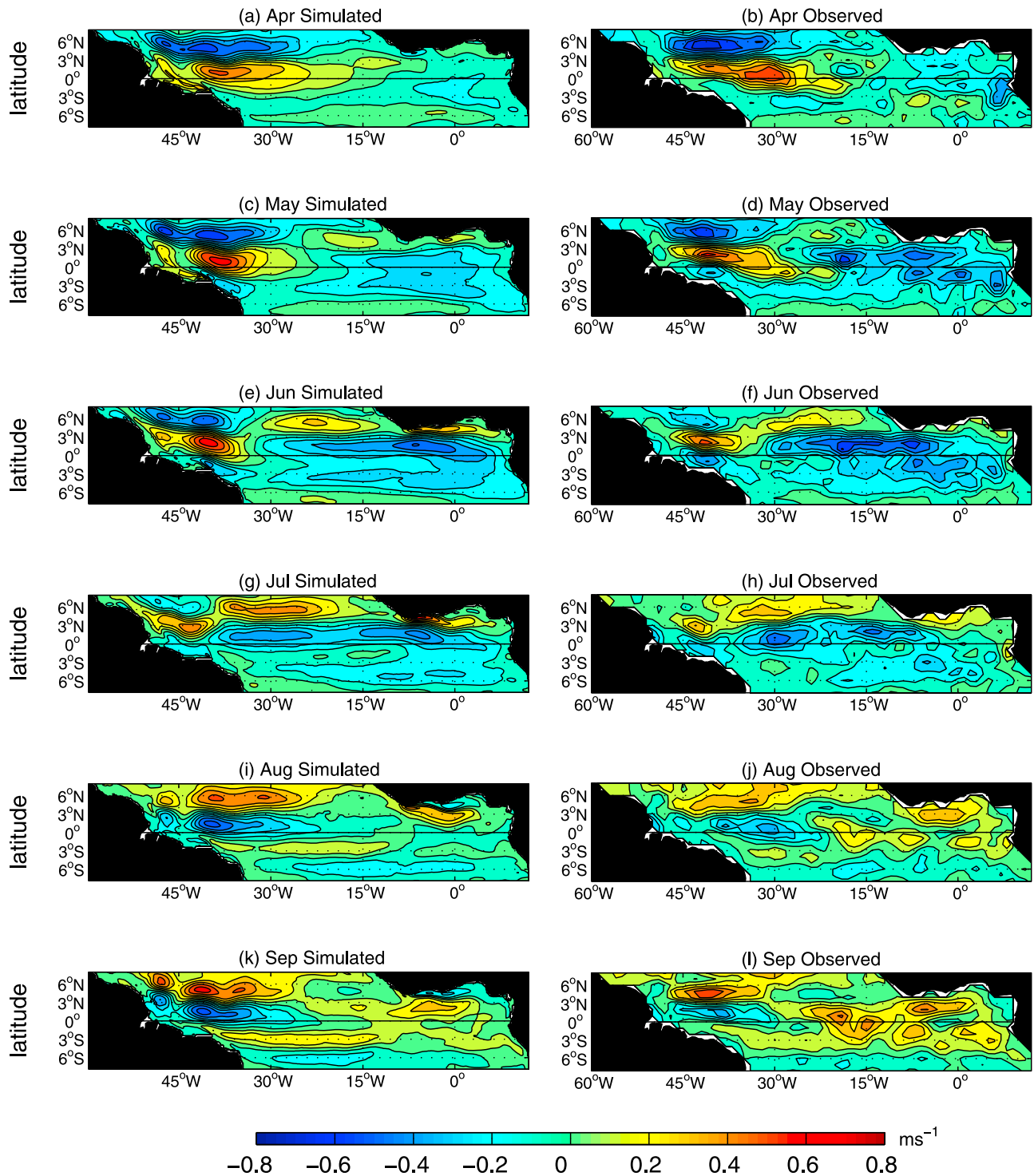


Figure 15. Monthly maps illustrating the spatial structure in climatological zonal surface current perturbations from the annual mean (ms^{-1}) over the tropical Atlantic between April and September. (a, c, e, g, i and k) Output from the ROMS-TAtl simulation (1980–2004), and (b, d, f, h, j and l) the surface current climatology product of Lumpkin and Garraffo [2005].

with the development and decay of the cold tongue between April and September. In May, westward surface currents within the central-eastern equatorial Atlantic are accelerated (Figures 15c) and these zonal surface current anomalies propagate westwards (Figures 15c, 15e, 15g, 15i and 15k). This westward propagation of zonal surface current anomalies

was attributed to first meridional mode Rossby waves by Ding *et al.* [2009] who found these to outweigh the Kelvin wave contribution. The westward propagation of zonal wind forcing is also thought to reinforce this westward propagation [Ding *et al.*, 2009]. The upwelling equatorial Kelvin waves (downwelling off-equatorial Rossby waves) are then

reflected at the eastern and western boundaries and act to decelerate westward surface currents near the equator between July and October (Figures 15g, 15j and 15k) [Ding *et al.*, 2009]. This decelerated westward surface flow captures the net effect is the delayed negative ocean memory feedback as it decreases the ability of winds to do work on the tropical Atlantic.

[62] This seasonally active delayed negative feedback is associated with a recharge of equatorial zonal mean heat content (a decrease in BPE). Figure 16a depicts seasonal changes in the BPE of the equatorial and tropical domains. BPE changes within these two regions are seen to be approximately in-phase with the exception that tropical BPE values peak approximately a month later than that in the equatorial Atlantic. As with APE, this result is ascribed to the fact that this larger domain takes longer to adjust than the equatorial region to seasonal changes in the wind forcing.

[63] Seasonal changes in the mass and BPE of the equatorial and tropical Atlantic regions are in-phase with seasonal changes in their heat content [Burls, 2010]. This relationship between heat content, mass and BPE suggests first, that seasonal variability in the density field appears to be primarily determined by seasonal variability in the temperature field, and secondly, that seasonal BPE change are primarily the result of seasonal changes in the mass of the equatorial and tropical domains rather than seasonal changes in vertical stratification due to mixing. These suggestions are reinforced by the results illustrated in Figure 16 which depicts the climatological balance of terms for the BPE evolution equation (equation (A3)). For the tropical and equatorial domains, the relative contribution of BPE changes due the advection of the density field, $\Phi_{bpa,r}$ versus BPE changes due to the combined effects of density diffusion and the penetrative solar radiation flux, $\Phi_{bpd,cl}$ is shown in Figure 16. Also shown is the portion of $\Phi_{bpd,cl}$ due to seasonal changes in surface buoyancy forcing ($\Phi_{bpd,cl}^{surfacebuoyancy}$ - note this term includes the penetrative solar radiation flux). The rather small residual between $\Phi_{bpd,cl}$ and $\Phi_{bpd,cl}^{surfacebuoyancy}$ (not shown) represents seasonal changes in BPE due to mixing within the domain and diffusion at the horizontal and bottom surfaces of the domain.

[64] For both the equatorial and tropical domains, seasonal BPE fluctuations are driven predominantly by fluctuations in the advection of the density field and secondly by fluctuations in the surface buoyancy forcing (Figure 16). BPE changes driven by the combined effects of mixing within the domain and diffusion at the horizontal and bottom surfaces of the domain are relatively small. Advection of the density field acts to increase BPE throughout the year for the tropical domain with values reaching a minimum (near zero) between July and October. For the equatorial domain, advection of the density field acts to increase BPE between November-July and decrease BPE between July and October. In both domains, the surface buoyancy forcing term reaches a minimum in March/April when surface heating over the respective domains is at its annual maximum and a maximum in June/July when surface heating is at its minimum (Figure 16).

[65] The results obtained here point to the fact that the decay of the cold tongue in the Atlantic is due to the delay associated with planetary wave propagation as the effect of transients on surface currents affects the ability of the wind

to do work on the ocean. As seen interannually in the Pacific, this seasonally active delayed negative feedback is associated with a recharge of equatorial zonal mean heat content and hence equatorial BPE changes are driven predominantly by fluctuations in the advection of the density field.

4. Discussion

[66] The seasonal cycle is a forced oscillation. However, between the months of April and October, seasonally excited coupled ocean-atmosphere interaction within the central-eastern Pacific and Atlantic basins results in a response which deviates from seasonal solar forcing [Mitchell and Wallace, 1992]. As in the Pacific, an asymmetric SST-mode, excited in April/May, leads to the growth of asymmetric conditions as the cold tongue-ITCZ complex develops in the Atlantic [Chang and Philander, 1994]. Unlike in the Pacific, the results presented above suggest that in the tropical Atlantic this process is accompanied by the excitation of a coupled mode with similar properties to the delayed oscillator mode operating interannually in the Pacific. As suggested by Ding *et al.* [2009], the term ‘thermocline mode’ is used to refer to this mode, as unlike the delayed oscillator mode, this mode occurs amidst seasonal forcing and is therefore different from the delayed oscillator idealization which describes a free mode of the coupled system.

[67] The results obtained suggest that the Bjerknes feedback is seasonally excited in April/May, resulting in the steep seasonal increase in equatorial Atlantic APE and associated decline in central-eastern basin SST (Figure 10). This positive feedback is then damped by a delayed negative feedback mechanism, similar to the negative feedback mechanism operating interannually in the Pacific. To summarize the behavior of this seasonally excited thermocline mode, Figure 17 displays a phase diagram between the two key variables, namely seasonal APE and the wind power values. In the Pacific, the presence of free oscillations associated with the delayed oscillator mode results in an out of phase relationship between wind power and APE on interannual timescales [Fedorov, 2007]. This out of phase relationship is due to the fact that APE changes are driven predominately by wind power and wind power displays a dependence on APE via its relationship with surface current anomalies and the ability of the wind to do work on the ocean. This in-quadrature relationship between wind power and APE observed interannually in the Pacific results in a phase diagram with wind power on the horizontal axis and APE on the vertical axis [Fedorov, 2007]. As seen in the corresponding phase diagram for the seasonal cycle in the Atlantic (Figure 17), only between April-September is a circular relationship evident between APE and the wind power term. It is during these months that the seasonally excited thermocline mode of coupled variability plays an active role in the tropical Atlantic’s seasonal cycle.

[68] The fact that the development of the cold tongue is accompanied by the excitation of a thermocline mode in the Atlantic and not the Pacific, results in several distinctions between the seasonal cycle in Atl3 SST and those in Niño3.4 and Niño3. These distinctions are illustrated in

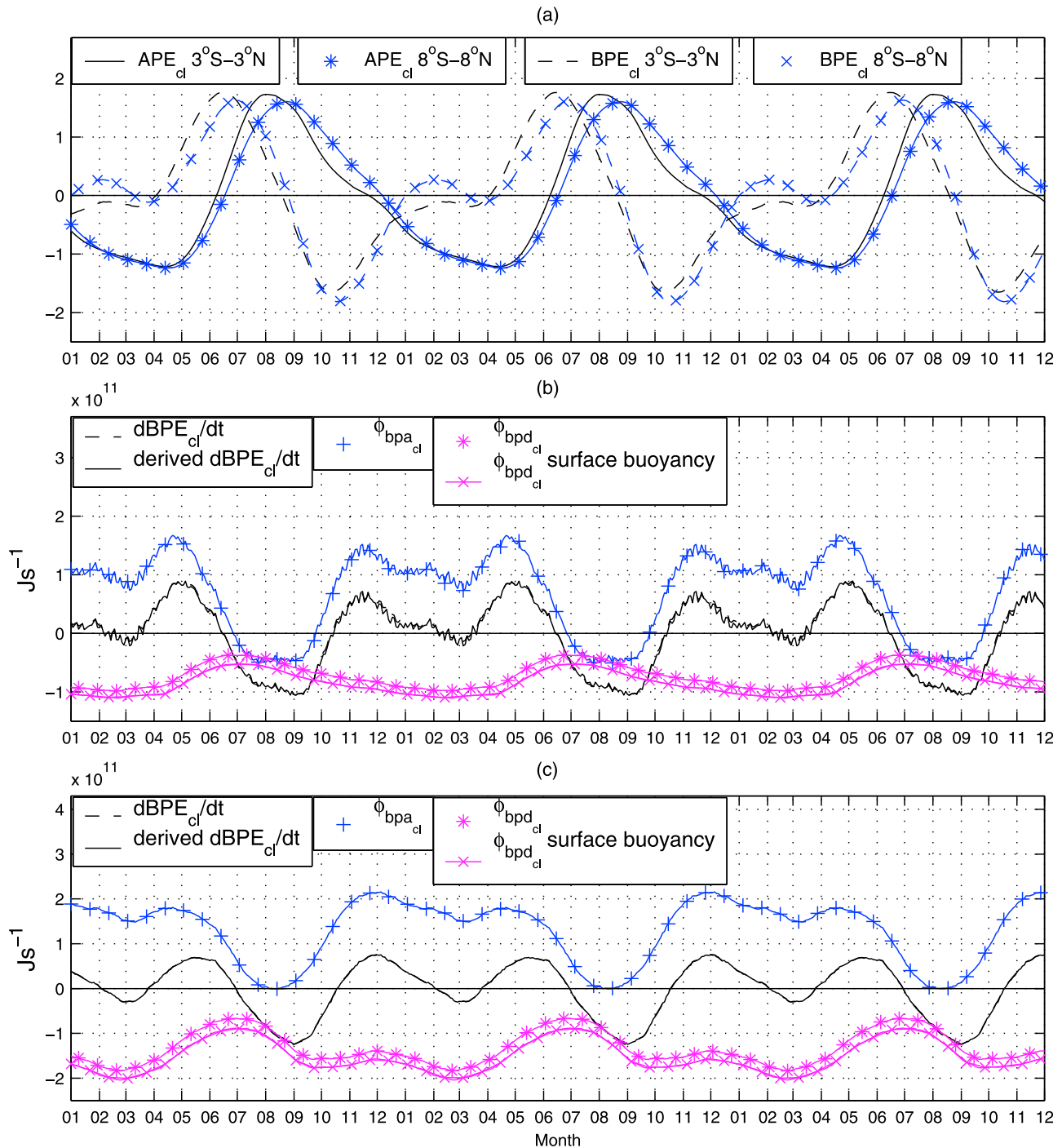


Figure 16. (a) Equatorial Atlantic (3°S–3°N 60°W–15°E 0–400 m) climatological APE and BPE changes versus tropical Atlantic (8°S–8°N 60°W–15°E 0–400 m) climatological APE and BPE changes. Values have been normalized to facilitate a better comparison. The climatological balance of terms (Js^{-1}) for the BPE evolution equation, assessed over (b) the equatorial Atlantic domain and (c) the tropical Atlantic domain. Following equation (A3), Φ_{bpa} represents BPE changes due to the advection of the density field, Φ_{bpd} BPE changes due to the combined effects of density diffusion and the penetrative solar radiation flux and $\Phi_{bpd_{cl}}^{surface\ buoyancy}$ is the portion of $\Phi_{bpd_{cl}}$ due to seasonal changes in surface buoyancy forcing. A 14 day running mean has been applied to the time series to smooth out the high frequency variability.

Figure 18, which compares seasonal variability in the Niño 3.4, Niño 3 and Atl3 SST indices. Seasonal cooling associated with the development of the equatorial cold tongue in the Atlantic is steeper and greater than in the

Pacific. This sharper, enhanced seasonal decline in central-eastern basin SST is attributed to the fact that the seasonally excited growth of asymmetric conditions about the equator is accompanied by a seasonally excited Bjerknes feedback as

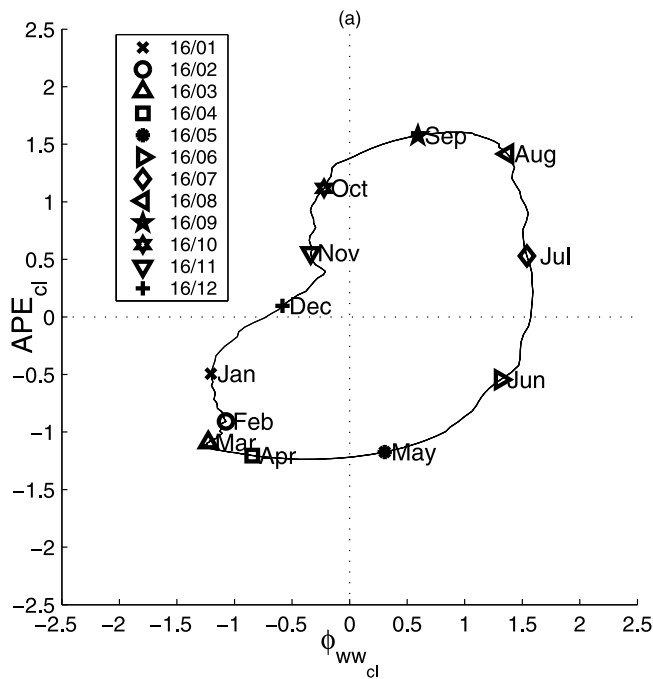


Figure 17. APE versus wind power phase diagram associated with the seasonal cycle in the tropical Atlantic domain (8°S–8°N 60°W–15°E). Values have been normalized and a 14 day running mean has been applied to the time series to smooth out the high frequency variability.

the thermocline shoals seasonally in the Atlantic. Secondly, cool conditions do not persist as long in the Atlantic as they do in the Pacific. Once established, the equatorial cold tongue-ITCZ complex in the Pacific sustains itself until December even as the region of maximum insolation and continental convection moves southwards. Only towards the end of the southern hemisphere summer does insolation manage to warm south equatorial SST enough to weaken the cold tongue-ITCZ complex allowing the ITCZ to migrate southwards back towards the equator [Chang and Philander, 1994]. In the Atlantic, cold conditions are not as stable as the rapid seasonal cooling abates in August and warming commences in September (Figure 18). This seasonal warming, which cuts short the cool period in the Atlantic, is seen to be in-phase with a deepening of the thermocline in the east as APE increases from August, a remotely forced thermocline depth influence absent from the Pacific.

[69] The APE-wind power perspective of coupled equatorial variability in the Pacific lends itself to the delayed-oscillator paradigm as the effect of transients on surface currents and hence the ability of the wind to do work on the ocean is seen as the delayed negative feedback mechanism [Goddard and Philander, 2000]. Interannually in the Pacific, thermocline perturbations associated with off-equatorial Rossby waves arriving in the west during the transition from one phase of ENSO to the next, affect surface currents and hence the ability of the wind to do work on the ocean, consistent with the delayed oscillator theory [Goddard and Philander, 2000]. Similarly, the results of the energetics analysis presented here lend themselves to the perspective that the delayed negative feedback mechanism, responsible for the decay of the cold tongue in the Atlantic, is due to the

delay associated with planetary wave propagation. The ENSO energetics analysis of Goddard and Philander [2000] captures the delayed negative feedback role of ocean memory within the mean perturbation wind power term which represents the effects of surface current fluctuations on the ability of the wind to do work on the ocean. It is shown in section 3.3 that this ocean memory mechanism is seasonally active and acts as the delayed, negative feedback process responsible for the decay of the seasonally excited Bjerknes feedback in the Atlantic between August and October. This result points to the fact that the ocean memory mechanism operates on much shorter timescales in the Atlantic than in the Pacific.

[70] As seen interannually in the Pacific, this seasonally active delayed negative feedback is associated with a recharge of equatorial zonal mean heat content. The results obtained in section 3.3 suggest that seasonal changes in the BPE of the equatorial and tropical Atlantic domains are controlled by seasonal changes in the warm water formation (surface buoyancy forcing) and escape (largely controlled by off-equatorial wind stress curl) [Lee and Csanady, 1999; Bunge and Clarke, 2009]. Seasonal changes in the advection of the density field for the tropical domain are consistent with observed seasonal changes in the escape of heat across 8°N regulated by changes in the NBC/NECC current system in response to the annual migration of the ITCZ [Lee and Csanady, 1999]. The 8°S–8°N region exports heat for most of the year acting to increase BPE, except between July–October when northward transport is blocked as the NBC veers offshore to feed the NECC and increased wind stress curl causes the mixed layer to deepen south of the NECC (8°N) and shoal to the north [Philander and Pacanowski, 1986b; Lee and Csanady, 1999]. For the equatorial domain, advection of the density field acts to increase BPE between November–July and decrease BPE between July and October, consistent with variability in the cross-latitude flux of warm surface waters forced by off equatorial wind stress curl [Bunge and Clarke, 2009].

[71] As seen in Figure 16a, seasonal APE and BPE changes are out of phase. This result is in agreement with the finding of Bunge and Clarke [2009] that changes in the slope of the equatorial thermocline are in-quadrature with variations in the amount of warm water above the thermocline between 2°N–2°S. The explanation for this relationship

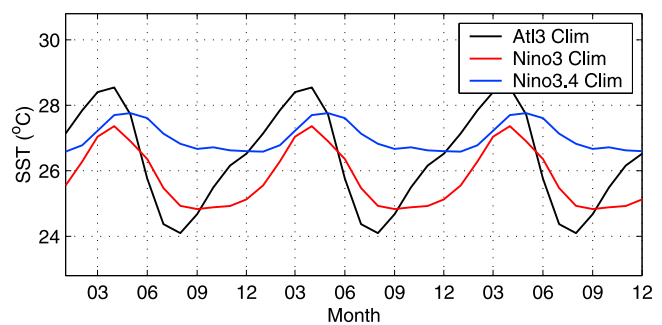


Figure 18. A comparison between seasonal variability in Niño 3.4 (5°N–5°S 170°W–120°W) SST, Niño 3 (5°N–5°S 150°W–90°W) SST, and Atl3 (3°S–3°N 20°W–0°E) SST. Created using monthly SODA data. SST values are given in °C.

provided by *Bunge and Clarke* [2009] is akin to that for the equivalent relationship observed in the Pacific on interannual timescales, namely the equatorial heat content recharge-discharge mechanism of *Jin* [1997]. The out of phase relationship seen between zonal slope of the equatorial thermocline (APE) and the mean depth of the equatorial thermocline (BPE) arises via the fact that they are both related to changes in the intensity of zonal wind stress near the equator: APE changes are associated with wind power changes and BPE changes are associated with wind stress curl changes. As revealed by the results of the seasonal APE evolution analysis described in section 3.2.1, seasonal BPE changes do not directly influence seasonal APE changes and their out of phase relationship arises from the fact that they are both related to seasonal changes in the intensity of zonal wind stress at the equator. While seasonal BPE changes do not directly influence seasonal APE changes the shallow mean depth of the thermocline within the equatorial region in April, May and June could potentially act in favor of the seasonal excitation of the Bjerknes feedback by preconditioning the region.

5. Conclusions

[72] Although time-averaged conditions above the tropical Atlantic and Pacific Oceans have similar trade winds and patterns of cloudiness and rainfall, and in the oceans similar currents and thermal structures, the two oceans have striking differences in their variability. In the eastern tropical Pacific, large changes in SST are highly correlated with changes in the depth of the thermocline on interannual but not on seasonal time-scales. The ocean-atmosphere interactions that determine the oscillations between El Niño and La Niña are entirely different from those that influence the seasonal cycle. In the Atlantic, on the other hand, the seasonal cycle involves substantial vertical movements of the thermocline and while seasonal SST fluctuations are large, interannual variations in the Atlantic are modest in amplitude.

[73] The results obtained within this paper suggest that these distinctions between the two basins are due to the fact that while the Bjerknes feedback and the delayed ocean memory mechanism act on interannual timescales in the Pacific, they act on seasonal timescales in the Atlantic. Unlike in the Pacific, where a new mechanism is introduced at interannual timescales in the form of basin wide thermocline depth adjustment, this is not the case in the Atlantic as the largest APE changes occur seasonally. This difference is thought to be due to the fact that the width of the Atlantic is less than a third of the Pacific, reducing the timescale of oceanic adjustment and allowing the oceanic response in the equatorial Atlantic to be closer to equilibrium with the seasonal forcing [*Philander and Pacanowski*, 1981; *Cane and Moore*, 1981; *Merle and Arnault*, 1985].

[74] Based on the relationship between SST, thermocline depth and surface zonal currents, *Ding et al.* [2009] suggest that the mechanism behind seasonal SST changes in the Atlantic is more consistent with the presence of a ‘thermocline mode’ than a SST-mode. The results obtained within this paper support this suggestion and raise the question: Is interannual SST variability associated with the zonal mode best explained in terms of a modulation of this newly identified, seasonally active thermocline mode? This question is

the focus of a coming paper (N. Burls et al., Energetics of the tropical Atlantic zonal mode, manuscript in preparation, 2011) in which the analysis has been extended to the interannual SST variations. The findings presented by *Burls* [2010] as well as the recent results of *Foltz and McPhaden* [2010a, 2010b] appear to support this framework in which to interpret coupled interannual variability within the equatorial Atlantic.

Appendix A: APE, BPE and KE Evolution Equations

[75] *Burls* [2010] derived an evolution equation for APE as defined by equation (2) such that terms are decomposed in a manner relevant to diagnosing equatorial ocean dynamics in an open boundary domain

$$\begin{aligned}
 \frac{dAPE}{dt} &= \underbrace{\int \int \int g \tilde{\rho} w dV}_{\Phi_{apk}} - \underbrace{\oint \left(-g \int_{\rho^*}^{\rho} (z_*(\rho') - z) d\rho' \right) \mathbf{u} \cdot \hat{n} dS}_{\Phi_{apa}} \\
 &+ \underbrace{\int \int \int g (-\alpha \nabla \cdot \gamma_t + \beta \nabla \cdot \gamma_s - \alpha Q_t) (z - z_*) dV}_{\Phi_{apd}} \\
 &= \underbrace{\int \int \int g \tilde{\rho} w dV}_{\Phi_{apk}} - \underbrace{\oint APE_{local} \mathbf{u} \cdot \hat{n} dS}_{\Phi_{apa}} \\
 &+ \underbrace{\int \int \int g (-\alpha \nabla \cdot \gamma_t + \beta \nabla \cdot \gamma_s - \alpha Q_t) (z - z_*) dV}_{\Phi_{apd}}, \tag{A1}
 \end{aligned}$$

where $\tilde{\rho}(\mathbf{x}, t)$ represents density perturbations from the reference state density $\rho^*(z, t) = \rho(z^*, t)$, such that $\rho = \rho^*(z, t) + \tilde{\rho}(\mathbf{x}, t)$. $\gamma_t = K_{th} \frac{\partial T}{\partial x} + K_{th} \frac{\partial T}{\partial y} + K_{tv} \frac{\partial T}{\partial z}$ where K_{th} represents the horizontal temperature diffusion coefficient and K_{tv} the vertical temperature diffusion coefficient. $\gamma_s = K_{sh} \frac{\partial S}{\partial x} + K_{sh} \frac{\partial S}{\partial y} + K_{sv} \frac{\partial S}{\partial z}$ where K_{sh} represents the horizontal salinity diffusion coefficient and K_{sv} the vertical salinity diffusion coefficient. Q_t represents subsurface heating due the penetration of the solar radiative flux. α and β are the temperature and salinity expansion coefficients respectively. $\mathbf{u} = (u, v, w)$ represents the full three dimensional velocity field and $-g \int_{\rho^*}^{\rho} (z_*(\rho') - z) d\rho' = APE_{local}$ is a local definition for APE [*Holliday and McIntyre*, 1981; *Molemaker and McWilliams*, 2010]. The derivation of this evolution equation is based on the assumption that a linear equation of state can be used to approximate density, thereby ensuring that the density field is conserved. An evolution equation for the global APE definition given by equation (2) has been previously derived [*Winters et al.*, 1995; *Huang*, 1998]. However these studies have focused on somewhat different physical processes and have dealt with closed domains. The above APE evolution equation has been derived such that terms are decomposed in a manner relevant to this paper’s focus on equatorial ocean dynamics in an open boundary equatorial domain.

[76] In the form given by equation (A1), the temporal evolution of APE within a fluid volume is driven by three terms: (1) Φ_{apk} is the buoyancy power term which is a reversible exchange term with the KE evolution equation (equation (A2)). (2) Φ_{apa} is the advection of local APE across the surfaces of the volume. (3) Φ_{apd} is APE changes

due to the combined effects of, changes in PE due to mixing within the domain, the rate of change of BPE driven by diapycnal mixing, and changes in APE due to the surface buoyancy flux [Winters *et al.*, 1995; Huang, 1998].

[77] To identify the primary physical processes contributing to the buoyancy power term, Φ_{apk} , which is the reversible exchange term between APE and KE, the balance of terms in the KE evolution equation is evaluated. The KE evolution equation is standard [Winters *et al.*, 1995; Goddard and Philander, 2000]

$$\begin{aligned} \frac{dKE}{dt} = & - \underbrace{\oint_{\Phi_{ka}} \left(\frac{\rho_o}{2} \mathbf{v}^2 \mathbf{u} \right) \cdot \hat{n} dS}_{\Phi_{ka}} - \underbrace{\oint_{\Phi_{pw}} (\tilde{p} \mathbf{u}) \cdot \hat{n} dS}_{\Phi_{pw}} - \underbrace{\int \int \int \tilde{\rho} g w dV}_{\Phi_{apk}} + \underbrace{\int \int_{z=0} \mathbf{v} \cdot \boldsymbol{\tau}_s dS}_{\Phi_{wv}} \\ & - \underbrace{\int \int \int \rho_o \left(K_{mh} \left(\frac{\partial \mathbf{v}}{\partial x} \cdot \frac{\partial \mathbf{v}}{\partial x} \right) + K_{mh} \left(\frac{\partial \mathbf{v}}{\partial y} \cdot \frac{\partial \mathbf{v}}{\partial y} \right) + K_{mv} \left(\frac{\partial \mathbf{v}}{\partial z} \cdot \frac{\partial \mathbf{v}}{\partial z} \right) \right) dV}_{\Phi_{ss}}, \end{aligned} \quad (\text{A2})$$

where ρ_o is the constant reference density. $\mathbf{v} = (u, v)$ the horizontal velocity field as vertical velocities do not contribute to KE under the hydrostatic assumption. K_{mh} is the horizontal viscosity coefficient and K_{mv} the vertical viscosity coefficient. $\tilde{p}(\mathbf{x}, t)$ represents pressure perturbations from the pressure field $p^*(z, t)$ in which all pressure surfaces are level and in hydrostatic balance with $\rho^*(z, t)$, such that $p = p^*(z, t) + \tilde{p}(\mathbf{x}, t)$. $\boldsymbol{\tau}_s$ is the surface wind stress.

[78] In this form, the temporal evolution of KE within a fluid volume is driven by five terms: (1) Φ_{ka} is the advection of KE across the surfaces of the volume. (2) Φ_{pw} is pressure work across the surfaces of the volume [Winters *et al.*, 1995]. (3) Φ_{apk} is the buoyancy power term which is a reversible exchange term with the APE evolution equation (equation (A1)). (4) Φ_{wv} is work done by the wind stress acting on surface currents [Goddard and Philander, 2000]. (5) Φ_{ss} is work done by shear stresses of horizontal flows within the domain [Winters *et al.*, 1995].

[79] The evolution equation for BPE is defined as

$$\begin{aligned} \frac{dBPE}{dt} = & - \underbrace{\int \int \int \mathbf{g} \mathbf{u} \cdot \nabla (-\alpha T + \beta S) z_* dV}_{\Phi_{bpa}} \\ & + \underbrace{\int \int \int \mathbf{g} (-\alpha \nabla \cdot \boldsymbol{\gamma}_t + \beta \nabla \cdot \boldsymbol{\gamma}_s - \alpha Q_t) z_* dV}_{\Phi_{bpd}}. \end{aligned} \quad (\text{A3})$$

[80] In this form, the temporal evolution of BPE within a fluid volume is driven by two terms: (1) Φ_{bpa} is BPE changes due to the advection of the density field. (2) Φ_{bpd} is BPE changes due to density diffusion as well as the penetrative solar radiation flux.

[81] **Acknowledgments.** This work emanates from the first author's PhD research and has been supported by resources and funding from the NRF, SANAP, the NRF/CNRS/French Embassy Doctoral Support Programme, the Centre for High Performance Computing and the Post-graduate Funding Office at the University of Cape Town, all of which are gratefully acknowledged. The first author would like to thank and acknowledge her Ph.D. examiners, as well as the reviewers of this paper, for their constructive feedback. We would like to thank the TAO Project Office of NOAA/PMEL for providing the PIRATA data used in this study <http://www.pmel.noaa.gov/tao/> as well as note that the SODA data of Carton and Giese [2008] was downloaded from <http://iridl.ldeo.columbia.edu/SOURCES/.CARTON-GIESE/.SODA/.v2p0p2-3/> and the surface current

climatology product of Lumpkin and Garraffo [2005] is available at http://www.aoml.noaa.gov/phod/dac/drifter_climatology.html.

References

- Adamec, D., and J. J. O'Brien (1978), The seasonal upwelling in the Gulf of Guinea due to remote forcing, *J. Phys. Oceanogr.*, *8*, 1050–1060.
- Barreiro, M., P. Chang, L. Ji, R. Saravanan, and A. Giannini (2005), Dynamical elements of predicting boreal spring tropical Atlantic sea-surface temperatures, *Dyn. Atmos. Oceans.*, *39*, 61–85.
- Battisti, D. S. (1988), Dynamics and thermodynamics of a warming event in a coupled tropical atmosphere-ocean model, *J. Atmos. Sci.*, *45*, 2889–2919.
- Battisti, D. S., and A. C. Hirst (1989), Interannual variability in a tropical atmosphere-ocean model: Influence of the basic state, ocean geometry and nonlinearity, *J. Atmos. Sci.*, *46*, 1687–1712.
- Biasutti, M., D. Battisti, and E. Sarachik (2005), Terrestrial influence on the annual cycle of the Atlantic ITCZ in an AGCM coupled to a slab ocean model, *J. Clim.*, *18*(1), 211–228.
- Bjerknes, J. (1969), Atmospheric teleconnections from the equatorial Pacific, *Mon. Weather Rev.*, *97*, 163–172.
- Brainerd, K. E., and M. C. Gregg (1995), Surface mixed and mixing layer depths, *Deep-Sea Res.*, *42A*(9), 1521–1543.
- Brown, J. N., and A. V. Fedorov (2010), How much energy is transferred from the winds to the thermocline on ENSO timescales?, *J. Clim.*, *23*(6), 1563–1580.
- Bunge, L., and A. J. Clarke (2009), Seasonal propagation of sea level along the equator in the Atlantic, *J. Phys. Oceanogr.*, *39*, 1069–1073.
- Burls, N. J. (2010), The role of ocean dynamics within tropical Atlantic climate variability, Ph.D. thesis, 225 pp., Univ. of Cape Town, Cape Town, South Africa.
- Busalacchi, A. J., and J. Picaut (1983), Seasonal variability from a model of the tropical Atlantic Ocean, *J. Phys. Oceanogr.*, *13*(9), 1564–1588.
- Cane, M. A., and D. W. Moore (1981), A note on low-frequency equatorial basin modes, *J. Phys. Oceanogr.*, *11*, 1578–1584.
- Carton, J. A., and B. S. Giese (2008), A reanalysis of ocean climate using Simple Ocean Data Assimilation (SODA), *Mon. Weather Rev.*, *136*, 2999–3017.
- Carton, J. A., and Z. X. Zhou (1997), Annual cycle of sea surface temperature in the tropical Atlantic Ocean, *J. Geophys. Res.*, *102*, 27,813–27,824.
- Carton, J. A., G. A. Chepurin, X. Cao, and B. S. Giese (2000), A Simple Ocean Data Assimilation analysis of the global upper ocean 1950–95. Part I: Methodology, *J. Phys. Oceanogr.*, *30*, 294–309.
- Chang, P. (1993), Seasonal cycle of sea surface temperature and mixed layer heat budget in the tropical Pacific Ocean, *Geophys. Res. Lett.*, *20*, 2079–2082.
- Chang, P. (1994), A study of seasonal cycle of sea surface temperature in the tropical Pacific Ocean using reduced gravity models, *J. Geophys. Res.*, *99*, 7725–7741.
- Chang, P., and G. Philander (1994), A coupled ocean-atmosphere instability of relevance to the seasonal cycle, *J. Atmos. Sci.*, *51*, 3627–3648.
- Chang, P., et al. (2006), Climate fluctuations of tropical coupled systems—The role of ocean dynamics, *J. Clim.*, *19*, 5122–5174.
- Ding, H., N. S. Keenlyside, and M. Latif (2009), Seasonal cycle in the upper equatorial Atlantic Ocean, *J. Geophys. Res.*, *114*, C09016, doi:10.1029/2009JC005418.
- du Penhoat, Y., and A. M. Treguier (1985), The seasonal linear response of the tropical Atlantic Ocean, *J. Phys. Oceanogr.*, *15*, 316–329.
- Fedorov, A. V. (2007), Net energy dissipation rates in the tropical ocean and ENSO dynamics, *J. Clim.*, *20*, 1108–1117.
- Fedorov, A. V., S. L. Harper, S. G. H. Philander, B. Winter, and A. Wittenberg (2003), How predictable is El Niño?, *Bull. Am. Meteorol. Soc.*, *84*, 911–919.
- Foltz, G. R., and M. J. McPhaden (2010a), Interaction between the Atlantic meridional and Niño modes, *Geophys. Res. Lett.*, *37*, L18604, doi:10.1029/2010GL044001.
- Foltz, G. R., and M. J. McPhaden (2010b), Abrupt equatorial wave-induced cooling of the Atlantic cold tongue in 2009, *Geophys. Res. Lett.*, *37*, L24605, doi:10.1029/2010GL045522.
- Foltz, G. R., S. A. Grodsky, J. A. Carton, and M. J. McPhaden (2003), Seasonal mixed layer heat budget of the tropical Atlantic Ocean, *J. Geophys. Res.*, *108*(C5), 3146, doi:10.1029/2002JC001584.
- Goddard, L., and S. G. H. Philander (2000), The energetics of El Niño and La Niña, *J. Clim.*, *13*, 1496–1516.
- Hayes, S. P., P. Chang, and M. J. McPhaden (1991), Variability of the sea surface temperature in the eastern equatorial Pacific during 1986–88, *J. Geophys. Res.*, *96*, 10,553–10,566.
- Hirst, A. C. (1986), Unstable and damped equatorial modes in simple coupled ocean-atmosphere models, *J. Atmos. Sci.*, *43*, 606–632.
- Holliday, D., and M. E. McIntyre (1981), On potential energy density in an incompressible stratified fluid, *J. Fluid. Mech.*, *107*, 221–225.

- Huang, R. X. (1998), Mixing and available potential energy in a Boussinesq ocean, *J. Phys. Oceanogr.*, **28**, 669–678.
- Jackett, D. R., and T. J. McDougall (1995), Minimal adjustment of hydrographic profiles to achieve static stability, *J. Atmos. Oceanic Technol.*, **12**, 381–389.
- Jin, F. (1997), An equatorial ocean recharge paradigm for ENSO. Part I: Conceptual model, *J. Atmos. Sci.*, **54**, 811–829.
- Kanamitsu, M., W. Ebisuzaki, J. Woollen, S.-K. Yang, J. J. Hnilo, M. Fiorino, and G. L. Potter (2002), NCEP-DOE AMIP-II reanalysis (R-2), *Bull. Am. Meteorol. Soc.*, **83**, 1631–1643.
- Keenlyside, N. S., and M. Latif (2007), Understanding equatorial Atlantic interannual variability, *J. Clim.*, **20**, 131–142.
- Large, W. G., J. C. McWilliams, and S. C. Doney (1994), Oceanic vertical mixing: A review and a model with a nonlocal boundary layer parameterization, *Rev. Geophys.*, **32**, 363–403.
- Lee, S.-K., and G. T. Csanady (1999), Warm water formation and escape in the upper tropical Atlantic Ocean: 2. A numerical model study, *J. Geophys. Res.*, **104**, 29,573–29,590.
- Li, T., and S. G. H. Philander (1997), On the seasonal cycle of the equatorial Atlantic Ocean, *J. Clim.*, **10**, 813–817.
- Lorbacher, K., D. Dommenget, P. Niiler, and A. Kohl (2006), Ocean mixed layer depth: A subsurface proxy of ocean-atmosphere variability, *J. Geophys. Res.*, **111**, C07010, doi:10.1029/2003JC002157.
- Lorenz, E. N. (1955), Available potential energy and the maintenance of the general circulation, *Tellus*, **7**, 157–167.
- Lumpkin, R., and Z. Garraffo (2005), Evaluating the decomposition of tropical Atlantic drifter observations, *J. Atmos. Oceanic Technol.*, **22**, 1403–1415.
- Marchesio, P., J. C. McWilliams, and A. Shchepetkin (2001), Open boundary conditions for long-term integration of regional oceanic models, *Ocean Modell.*, **3**, 1–20.
- McPhaden, M. J., et al. (1998), The tropical ocean-global atmosphere observing system: A decade of progress, *J. Geophys. Res.*, **103**, 14,169–14,240.
- Menkes, C., J. Vialard, S. Kennan, J. Boulanger, and G. Madec (2006), A modeling study of the impact of tropical instability waves on the heat budget of the eastern equatorial Pacific, *J. Phys. Oceanogr.*, **36**, 847–865.
- Merle, J. (1980), Seasonal heat budget in the equatorial Atlantic Ocean, *J. Phys. Oceanogr.*, **10**, 464–469.
- Merle, J., and S. Arnault (1985), Seasonal variability of the dynamic topography in the tropical Atlantic Ocean, *J. Mar. Res.*, **43**, 267–288.
- Mitchell, T. P., and J. M. Wallace (1992), The annual cycle in equatorial convection and sea surface temperature, *J. Clim.*, **5**, 1140–1156.
- Molemaker, M. J., and J. C. McWilliams (2010), Local balance and cross-scale flux of available potential energy, *J. Fluid Mech.*, **645**, 295–314.
- Neelin, J. D. (1991), The slow sea surface temperature mode and the fast-wave limit: Analytic theory for tropical interannual oscillations and experiments in a hybrid coupled model, *J. Atmos. Sci.*, **48**, 584–606.
- Neelin, J. D., D. S. Battisti, A. C. Hirst, F. Jin, Y. Wakata, T. Yamagata, and S. E. Zebiak (1998), ENSO theory, *J. Geophys. Res.*, **103**(C7), 14,261–14,290.
- Okumura, Y., and S.-P. Xie (2004), Interaction of the Atlantic equatorial cold tongue and the African monsoon, *J. Clim.*, **17**, 3589–3602.
- Okumura, Y., and S.-P. Xie (2006), Some overlooked features of tropical Atlantic climate leading to a new Niño-like phenomenon, *J. Clim.*, **19**, 5859–5874.
- Oort, A. H., S. C. Ascher, S. Levitus, and J. P. Peixoto (1989), New estimates of the available potential energy in the world ocean, *J. Geophys. Res.*, **94**, 3187–3200.
- Peter, A., M. L. Henaff, Y. P. Y. du Penhoat, C. Menkes, F. Marin, J. Vialard, G. Caniaux, and A. Lazar (2006), A model study of the seasonal mixed layer heat budget in the equatorial Atlantic, *J. Geophys. Res.*, **111**, C06014, doi:10.1029/2005JC003157.
- Philander, S. G. H., and R. C. Pacanowski (1981), Response of equatorial oceans to periodic forcing, *J. Geophys. Res.*, **86**, 1903–1916.
- Philander, S. G. H., and R. C. Pacanowski (1986a), A model of the seasonal cycle in the tropical Atlantic Ocean, *J. Geophys. Res.*, **91**, 14,192–14,206.
- Philander, S. G. H., and R. C. Pacanowski (1986b), The mass and heat budgets in a model of the tropical Atlantic, *J. Geophys. Res.*, **91**, 14,212–14,220.
- Reid, R., B. Elliot, and D. Olson (1981), Available potential energy: A clarification, *J. Phys. Oceanogr.*, **11**, 15–29.
- Schouten, M. W., R. P. Matano, and T. P. Strub (2005), A description of the seasonal cycle of the equatorial Atlantic from altimeter data, *Deep-Sea Res.*, **52**, 477–493.
- Servain, J., A. Busalacchi, M. McPhaden, A. Moura, G. Reverdin, M. Vianna, and S. Zebiak (1998), A Pilot Research Moored Array in the Tropical Atlantic (PIRATA), *Bull. Am. Meteorol. Soc.*, **79**, 2019–2031.
- Shchepetkin, A., and J. McWilliams (2005), The regional oceanic modeling system (ROMS): A split-explicit, free-surface, topography-following-coordinate oceanic model, *Ocean Modell.*, **9**, 347–404.
- Sterl, A., and W. Hazeleger (2003), Coupled variability and air-sea interaction in the South Atlantic Ocean, *Clim. Dyn.*, **21**, 559–571.
- Suarez, M. J., and P. S. Schopf (1988), A delayed action oscillator for ENSO, *J. Atmos. Sci.*, **45**, 3283–3287.
- Swenson, M. S., and D. V. Hansen (1999), Tropical Pacific Ocean mixed layer heat budget: The Pacific cold tongue, *J. Phys. Oceanogr.*, **29**, 69–81.
- Vauclair, F., and Y. du Penhoat (2001), Interannual variability of the upper layer of the tropical Atlantic Ocean from in situ data between 1979 and 1999, *Clim. Dyn.*, **17**, 527–546.
- Vialard, J., and P. Delecluse (1998), An OGCM study for the TOGA decade. Part I: Role of salinity in the physics of the western Pacific fresh pool, *J. Phys. Oceanogr.*, **28**, 1071–1088.
- Wang, W., and M. J. McPhaden (1999), The surface-layer heat balance in the equatorial Pacific Ocean. Part I: Mean seasonal cycle, *J. Phys. Oceanogr.*, **29**, 1812–1931.
- Weingartner, T. J., and R. H. Weisberg (1991), A description of the annual cycle in sea surface temperature and upper ocean heat in the equatorial Atlantic, *J. Phys. Oceanogr.*, **21**, 83–96.
- Weisberg, R. H., and T. Y. Tang (1985), On the response of the equatorial thermocline in the Atlantic Ocean to the seasonally varying trade winds, *J. Geophys. Res.*, **90**(C4), 7117–7128.
- Weisberg, R. H., and T. Y. Tang (1987), Further studies on the response of the equatorial thermocline in the Atlantic Ocean to the seasonally varying trade winds, *J. Geophys. Res.*, **92**(C4), 3709–3727.
- Weisberg, R. H., and T. Y. Tang (1990), A linear analysis of equatorial Atlantic Ocean thermocline variability, *J. Phys. Oceanogr.*, **20**, 1813–1825.
- Winters, K. B., P. N. Lombard, J. J. Riley, and E. A. D'Asaro (1995), Available potential energy and mixing in density-stratified fluids, *J. Fluid Mech.*, **289**, 115–128.
- Xie, S. (1994), On the genesis of the equatorial annual cycle, *J. Clim.*, **7**, 2008–2013.
- Xie, S.-P., and J. A. Carton (2004), Tropical Atlantic variability: Patterns, mechanisms, and impacts, *Earth Climate: The Ocean-Atmosphere Interaction*, *Geophys. Monogr. Ser.*, vol. 147, pp. 121–142, edited by C. Wang, S.-P. Xie, and J. A. Carton, AGU, Washington, D. C.
- Xie, S.-P., and S. G. H. Philander (1994), A coupled ocean-atmosphere model of relevance to the ITCZ in the eastern Pacific, *Tellus A*, **46**, 340–350.
- Yu, X., and M. McPhaden (1999), Seasonal variability in the equatorial Pacific, *J. Phys. Oceanogr.*, **29**, 925–947.
- Zebiak, S. E. (1993), Air-sea interaction in the equatorial Atlantic region, *J. Clim.*, **6**, 1567–1586.
- Zebiak, S. E., and M. Cane (1987), A model El Niño–Southern Oscillation, *Mon. Weather Rev.*, **115**, 2262–2278.

N. J. Burls and C. J. C. Reason, Department of Oceanography, University of Cape Town, Private Bag X3, Rondebosch, Cape Town 7701, South Africa. (natalie.burls@uct.ac.za)

P. Penven, LPO, UMR 6523 CNRS, IFREMER, IRD, UBO, LMI ICEMASA, Centre IRD de Bretagne, BP 70, Plouzane F-29280, France.

S. G. Philander, Geophysical Fluid Dynamics Laboratory, Princeton University, Princeton University Forrestal Campus, 201 Forrestal Rd., Princeton, NJ 08540-6649, USA.